Journal of Bio- and Tribo-Corrosion (2025) 11:116
https://doi.org/10.1007/s40735-025-01032-6

Modelling the Corrosion Inhibition Efficiency of *Garcinia Cambogia* Extract on Mild Steel in Acid Media Using ANN and RSM Approaches

K. Vidhya Thomas[1,3] · K. Joby Thomas[2,3] · A. S. Sabu[4] · C. Sini Varghese[1,3] · Reeja Jhonson[3]

Received: 27 July 2025 / Revised: 25 August 2025 / Accepted: 28 August 2025 / Published online: 13 September 2025

Abstract

Garcinia cambogia extract (GCE) was employed as a green corrosion inhibitor, a sustainable alternative to toxic and non-biodegradable synthetic inhibitors, on mild steel in 1 M HCl and 0.5 M H_2SO_4. Corrosion inhibition efficiency of GCE was assessed using physicochemical, electrochemical, morphological, and quantum chemical techniques. Moreover, the effects of inhibitor concentration, acid concentration, and temperature on the inhibition efficiency (IE) were modelled and optimised by response surface methodology (RSM) and artificial neural network (ANN). Electrochemical studies revealed that GCE acts as a mixed type corrosion inhibitor. Kinetic and thermodynamic data suggested that GCE adsorbs onto the metal surface via both physisorption and chemisorption. Modelling of parameters using an artificial neural network (ANN) indicated that the model was trained effectively. The dual use of advanced computational modelling, RSM and ANN, along with their good agreement with experimental results, constitutes the novelty of this work. The future scope of this work involves testing GCE as a green corrosion inhibitor under real-world industrial conditions.

Keywords Corrosion inhibitor · GCE · Adsorption · EIS · ANN · RSM

1 Introduction

Metals have played a fundamental role in technological development and societal advancement from the very beginning of human civilization. Mild steel is a readily available and easily manufactured alloy found worldwide. Even though mild steel is highly susceptible to corrosion, it is an affordable material with low carbon content and minimal alloying elements [1]. Many industries, such as chemical engineering, mining, and oil and gas, operate in acidic environments where metals react with acids or other corrosive substances, causing the breakdown of their structure, weakening the material, and leading to gradual metal loss over time. Corrosion inhibitors are effective for protecting metals from deterioration when exposed to aqueous solutions, particularly in closed systems such as cooling and heating systems. In recent years, green chemistry principles have garnered significant attention owing to their role in the protection of metals from corrosion. Plant-based products are a rich source of numerous organic compounds that can donate lone pairs of electrons to metal surfaces. As a result, they can act as effective corrosion inhibitors and interact with metals either by chemisorption or physisorption [2]. The adsorptive layer formed on the metal surface protects the metal from acidic solution, thereby minimising corrosion. Natural products, such as plant extracts, can be used as green corrosion inhibitors because of their eco-friendliness, low cost, availability, and renewability. Many researchers have investigated natural plant products, such as leaves, seeds, roots, fruits, and flowers, as efficient and sustainable corrosion inhibitors on mild steel surfaces in aggressive acidic environments.

✉ K. Joby Thomas
drjobythomask@gmail.com

1 Department of Chemistry, Centre for Research in Chemical Sciences, St. Joseph's College (Autonomous), Irinjalakuda, Affiliated to University of Calicut, Thrissur, Kerala 680121, India

2 Amala Integrated Medical Research Department, Amala Institute of Medical Sciences, Thrissur, Kerala, India

3 Department of Chemistry, Centre for Electrochemical Studies, St. Thomas College (Autonomous), Thrissur, Affiliated to University of Calicut, Thrissur, Kerala 680001, India

4 Department of Mathematics, St. Thomas College (Autonomous), Thrissur, Affiliated to University of Calicut, Thrissur, Kerala 680001, India

Ghazal Sadat Sajadi and co-workers have been analysed the mild steel corrosion control in acidic solution by *Ranunculus arvensis* and *Glycine max* extracts as green inhibitors experimentally and theoretically in 2022 [3]. Aouatife Zaher et al. have been discovered *Ammi visnaga* L. extract as a green corrosion inhibitor in 1 M HCl for carbon steel using combined computational & electrochemical studies in 2022 [4]. In 2016, Anupama et al. [5], used gravimetric and electrochemical methods to investigate the corrosion behaviour of methanolic extracts of *Ruta graveolens* (RGE) leaves in 1 M HCl for mild steel. According to EIS tests, RGE demonstrated 98% inhibitory efficiency at 4% v/v. In 2020, Saxena et al. reported that ethanol extracts of fruits of *Tinospora cordifolia* showed 87.18% effectiveness at an inhibitor concentration of 500 mg/L using potentiodynamic polarisation studies [6]. In 2019, Saxena et al., [7] used surface morphological and electrochemical analyses to investigate the inhibitory power of ethanol extracts of *Terminalia chebula* seeds. In 0.5 M H_2SO_4, it demonstrated 94.07% inhibitory potency for low-carbon steel at 500 mg/L inhibitor concentration according to potentiodynamic polarisation experiments.

Recently, 'intelligence' approaches such as artificial neural networks (ANNs) and response surface methodology (RSM) are used to model and optimise metal corrosion inhibition performance. They are highly effective in modelling complex, nonlinear systems, making them ideal for predicting corrosion inhibition efficiency based on multiple input parameters. In corrosion studies, ANNs are employed to model the corrosion inhibition efficiency of inhibitors as a function of variables, such as concentration and temperature. Even with limited datasets, ANNs can provide reliable predictions of inhibition efficiency. Furthermore, they serve as effective tools for identifying the optimal conditions, such as inhibitor concentration and operating temperature, to maximise corrosion inhibition performance. Response surface methodology (RSM) is a mathematical and statistical approach that is useful for developing, improving, and refining process factors. It proposes evaluating a combination of many factors with few trials. Therefore, the optimisation of the process is time- and cost-effective. Many researchers have used ANNs and RSM to investigate the impact of various parameters on the system's properties and optimise the test parameters, reduce the corrosion rate, and elevate the inhibition efficacy. For example, Amodu et al. demonstrated that *Musa paradisiaca* peel extract acts as an eco-friendly corrosion inhibitor for mild steel in 1 M HCl using gasometric and thermometric methods [8]. In their study, Response Surface Methodology (RSM) and Artificial Neural Networks (ANNs) were employed as robust optimisation techniques. O. Oyewole, T.A. Oshin, and B.O. Atotuoma investigated the corrosion inhibition performance of *Corchorus olitorius* stems on mild steel in H_2SO_3, utilising both experimental methods and theoretical approaches, including ANNs and RSM [9]. Abdeslam Ansari and his team reported that *Ocimum basilicum* essential oil exhibited excellent corrosion mitigation efficiency for C38 steel in 0.5 M H_2SO_4, employing a combination of physicochemical analysis, electrochemical measurements, theoretical modelling, and optimization techniques [10]. In 2024, Ahmed E.S. and Mohan Ganesh G. discovered that *Azadirachta indica* leaves as eco-friendly corrosion inhibitor on TMT steel in 1 M HCl and 1 M NaCl media by applying experimental, spectroscopic, and artificial neural networks (ANN) [11]. In 2025, K. Krishnanjana and Mohan Ganesh G. applied *Punica granatum* peel powder as an effective green corrosion inhibitor on TMT steel in NaCl medium using electrochemical, spectroscopic, and artificial neural networks (ANN) [12].

This study presents the corrosion inhibition behavior of a non-toxic and environmentally benign inhibitor, *Garcinia cambogia* extract (GCE), for mild steel in 1 M HCl and 0.5 M H_2SO_4. The International Plant Names Index (IPNI) entry for Garcinia cambogia Desr. is recorded under the identifier LSID: urn:lsid:ipni.org:names:427866-1. In the Linnaean Herbarium, hosted by the Linnean Society of London (herbarium code: LINN), the specimen sheet LINN-HS857-2-1 corresponds to *Garcinia cambogia* in the Linnaean collection. The investigation employed a comprehensive set of corrosion analysis techniques, including physicochemical characterisation, electrochemical measurements, surface morphological studies, quantum mechanical calculations, ANN modelling, and RSM-based optimisation. Although the medicinal properties of *Garcinia cambogia* have been extensively studied, their corrosion resistance properties have not yet been thoroughly explored. This prompted the selection of *Garcinia cambogia,* a member of the Guttiferae family, as corrosion inhibitors. Although there are many bioactive substances present in *Garcinia cambogia* leaf extract, the main groups of chemicals are hydroxycitric acid (HCA) and hydroxycitric acid lactone (HCA lactone) [13]. The structures of HCA and HCA lactone are shown in Fig. 1. Acidic solutions are widely used in various industrial processes making HCl and H_2SO_4 suitable corrosive media for this study. Gravimetric and electrochemical

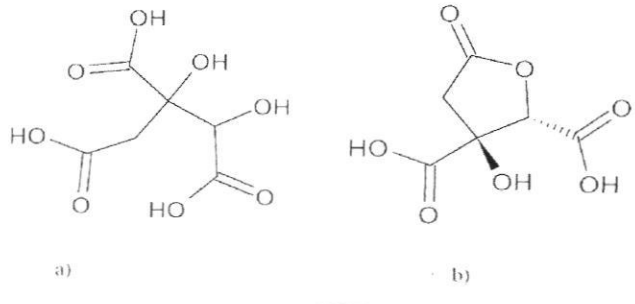

Fig. 1 Structure of **a** hydroxycitric acid, **b** hydroxycitric acid lactone

measurements were performed to evaluate the corrosion rate of mild steel with various concentrations of GCE at room temperature. Furthermore, employing response surface methodology (RSM) and artificial neural networks (ANN), the impacts of temperature, acid concentration, and GCE concentration on inhibitory efficiency were modelled and optimised.

Although several plant extracts have been utilized for their corrosion inhibition potential, *Garcinia cambogia* extract has not been explored for its inhibition efficiency on mild steel in HCl and H_2SO_4 media. In addition to conventional corrosion studies such as weight loss, electrochemical, and morphological analyses, the present work applies advanced computational tools—Artificial Neural Networks (ANN) and Response Surface Methodology (RSM)—to develop robust predictive models. Thus, this study bridges the gap between experimental observations and reliable predictive tools for practical industrial applications.

2 Materials and Methods

2.1 Preparation of GCE

Garcinia cambogia leaves were washed with clean water, shade dried, and ground into a fine powder. Powdered samples (5 g) were refluxed in 100 mL of ethanol for 4 h. The extract was filtered and excess solvent was removed through rotary evaporator [14]. The resulting extract was kept in an airtight container at 4 °C for further tests [15, 16]. For the experimental analysis, concentrations ranging from 1 to 5% (v/v) were prepared.

2.2 Preparation of Mild Steel Coupons

The mild steel used consists of 97.05% iron and 2.95% carbon. Metal sheets of mild steel were cut into 1 cm^2 coupons, which were then abraded sequentially using emery papers with grit sizes of 100, 220, 440, 800, 1000, 1500, and 2000. After the abrasion, the samples were rinsed with distilled water and acetone.

2.3 Preparation of Acidic Media

Merck-grade HCl and H_2SO_4 were used to prepare 1 M HCl and 0.5 M H_2SO_4 solutions, respectively. For the Weight loss measurements, 50 mL of each acid solution was used. The effect of temperature on corrosion inhibition efficiency was evaluated at elevated temperatures of 303, 313, 323, and 333 K.

2.4 FTIR Spectroscopy

FT-IR spectral analysis of the GCE was carried out using a Shimadzu IR Affinity-1 Fourier transform infrared (FT-IR) spectrophotometer.

2.5 Weight Loss Measurement

Weight loss measurements of mild steel coupons were conducted in both the presence and absence of GCE at concentrations ranging from 1 to 5 v/v% in two corrosive environments over a 24-h immersion period at varying temperatures. Prior to immersion, mild steel coupons were polished, measured, and Weighed. The prepared samples were then immersed in 1 M HCl and 0.5 M H_2SO_3 solutions, into which different concentrations (0–5 v/v%) of GCE were added. The solution was then left undisturbed for 24 h. GCE was completely soluble in both acidic media. After the immersion period, the metal coupons were removed, cleaned, dried, and re-weighed to determine their weight loss. Equation (1) is used to calculate the corrosion rate (υ) of mild steel [17]:

$$v = \frac{KW}{DSt} \tag{1}$$

where K = 87,600, W is the weight loss of the metal coupon (g), S is the total area of the coupon (cm^2), D is the density of the metal (g cm^{-3}), and t is the period of immersion (h). Based on the calculated corrosion rates, the inhibition efficiency (η%) of the GCE was determined using Eq. (2) [18]:

$$\eta\% = \frac{100(\upsilon_0 - \upsilon)}{\upsilon_0} \tag{2}$$

where υ_0 and υ indicate the corrosion rate of metal coupons immersed in acid solutions without and with GCE, respectively.

The Arrhenius Eq. (3) was used to compute the thermodynamic parameters for corrosion, including the Arrhenius parameter (A), activation energy for decay, entropy of corrosion (ΔS*), and enthalpy of corrosion (ΔH*).

$$K = A \exp\left(\frac{-E_a}{RT}\right) \tag{3}$$

where A is the Arrhenius parameter, a pre-exponential component, E_a is the activation energy for corrosion, R is the gas constant, T is the temperature, and K is the rate of corrosion. To determine the ΔS* and ΔH* values, Eqs. (4) and (5) were utilised [19].

$$K = \left(\frac{RT}{Nh}\right)\exp\left(\frac{\Delta S^*}{R}\right)\exp\left(\frac{-\Delta H^*}{RT}\right) \tag{4}$$

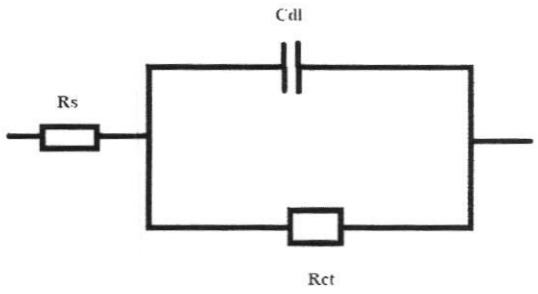

Fig. 2 Randle's circuit

$$\log\frac{K}{T} = \log\frac{R}{Nh} + \frac{\Delta S^{*}}{2.303\,R} - \frac{\Delta H^{*}}{2.303\,RT} \quad (5)$$

where *N* denotes the Avagadro number, and h is Planck's constant.

2.6 Electrochemical Analysis

An Ivium CompactStat electrochemical workstation equipped with IviumSoft software and a three-electrode electrochemical cell was employed for electrochemical analyses such as electrochemical impedance spectroscopy (EIS), potentiodynamic polarisation studies, and electrochemical noise studies. In the EIS and potentiodynamic polarisation studies, a traditional three-electrode setup was used, comprising a calomel electrode as the reference electrode, a platinum electrode as the counter electrode, and a mild steel electrode with an exposed surface area of 1 cm^2 as the working electrode. In the electrochemical noise experiments, two mild steel electrodes, each with exposed surface area of 1 cm^2, acted as the working and counter electrodes. All electrochemical analyses were conducted at room temperature with varying concentrations (1–5% v/v) of GCE added to the corrosive media.

The electrochemical workstation functioned over a frequency range of 1 kHz to 100 mHz with a scan rate of 10 mV/sec in EIS. Randle's circuit (Fig. 2) was employed as the equivalent circuit, consists of solution resistance (R_s), double layer capacitance (C_{dl}) and charge transfer resistance (R_{ct}) or polarization resistance (R_p). In the electrochemical cell, charge transfer process places the double layer capacitance parallel with the impedance. R_{ct} values extracted from the Nyquist plots were substituted to determine the corrosion inhibition efficiency of the GCE, calculated using Eq. (6) [20].

$$\eta\text{EIS}\,\% = \frac{100(R'_{ct} - R_{ct})}{R'_{ct}} \quad (6)$$

Here, R′ct and Rct refer to the charge-transfer resistance of the working electrode with and without GCE, respectively.

The open-circuit potential (OCP) method was utilised for potentiodynamic polarisation studies to examine the relationship between the current and potential for mild steel immersed in the test solution. The potential applied to the working electrode (mild steel) ranged from −250 to +250 mV, with a scan rate of 1 mV/s. The inhibition efficiency ($\eta_{pol}\%$) was determined using the corrosion current density (i_{corr}) values derived from the analysis of both anodic and cathodic polarization curves, according to Eq. (7) [5]:

$$\eta\text{pol}\% = \frac{100\left(i_{corr} - i'_{corr}\right)}{i_{corr}} \quad (7)$$

i_{corr} and i'_{corr} denote the corrosion current densities of the working electrode in the absence and presence of the GCE, respectively.

Alternatively, the corrosion inhibition efficiency can be determined from the polarisation resistance values using Eq. (8).

$$\eta_{Rp}\% = \frac{100\left(R'_p - R_p\right)}{R'_p} \quad (8)$$

where R'_p and R_p are the polarisation resistances with and without the GCE, respectively.

Electrochemical noise experiments were conducted for the period 1200 s.

2.7 Surface Morphological Studies

Surface morphology studies were conducted using (AFM; WITEC ALPHA300 RA). Mild steel coupons were immersed in 1 M HCl and 0.5 M H_2SO_4 solutions in the presence and absence of GCE for 24 h. Following the immersion period, the metal coupons were subjected to surface characterisation.

2.8 Quantum Chemical Calculations

Quantum chemical investigations of HCA and HCA lactone, the active components of GCE, have established its anti-corrosion behaviour. The mechanism of corrosion inhibition is explained by the interaction between the HOMO of the inhibitor (GCE) and LUMO of mild steel (Fe). A lower energy gap ($\Delta E = E_{LUMO} - E_{HOMO}$) indicates a higher tendency of the inhibitor to adsorb rapidly onto the metal surface [21]. The quantum chemical parameters were calculated using DFT with GAMESS software. The B3LYP function was employed as the correlation method and STO-3G was used as the basis set.

2.9 Artificial Neural Networks (ANN)

Inspired by the human brain, artificial neural networks (ANNs) are potent computational tools for solving complex and challenging issues in machine learning, data analysis, and pattern recognition. An ANN consists of input, hidden, and output layers that in turn receive, process, and forecast data [22]. The backpropagation method reduces the difference between the initial output and the ANN output.

The fundamental mathematical expressions for the neural network are as follows.

$y_m = \sum_{n=1}^{p} w_{mn} x_n + q_m$, x_n is the input, w_{mn} is the weight associated with the *nth* node to the *mth* hidden layer, q_m is the hidden *mth* layer bias [23]. The weights are modified during the training process.

Throughout the investigation, the Levenberg–Marquardt algorithm (LMA) was used for data validation, testing, and training. LMA's improved robustness, convergence rate, and speed of the LMA make it a good choice for neural-network training. Figure 3 shows the flow chart of the basic ANN algorithm.

The study used samples from the experimental investigation as input variables to train the artificial neural network. Temperature, HCl concentration, and GCE concentration were three distinct input nodes. The experimental inhibition efficiency samples were regarded as the output layers. Figure 4 shows the neural network model used to forecast the inhibition efficiency.

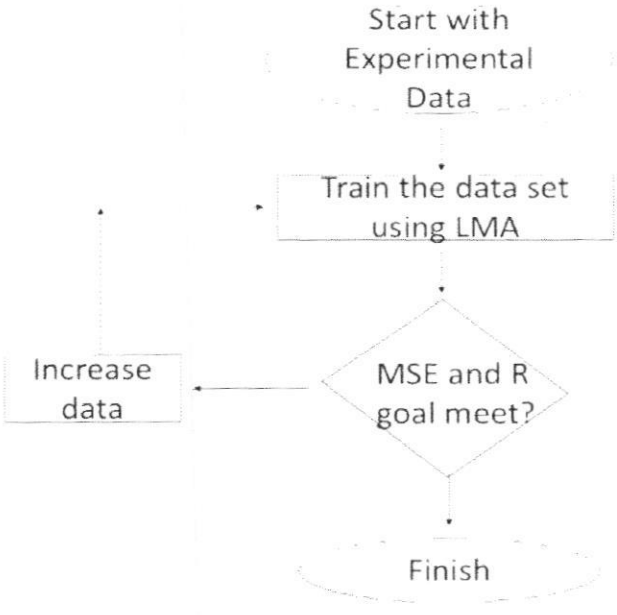

Fig. 3 Flow chart of ANN using LMA

2.10 Response Surface Methodology (RSM)

The response surface methodology (RSM) has emerged as a widely used optimisation technique in recent years. It is employed to analyse the influence of individual test factors and their interactions on a response variable and to develop an empirical model that predicts optimal process conditions [24]. In corrosion studies, RSM is used to determine the optimum parameter conditions to achieve maximum corrosion inhibition efficiency. In the present study, the Minitab 19 programming tool was used for the experimental design using the Box–Behnken design (BBD), which comprised 15 experimental runs. Three test factors were applied: X_1, temperature (K); X_2, GCE concentration (v/v %); and X_3, acid concentration, each evaluated at three levels, as outlined in Table 1.

Fig. 4 ANN Architecture for the prediction of IE

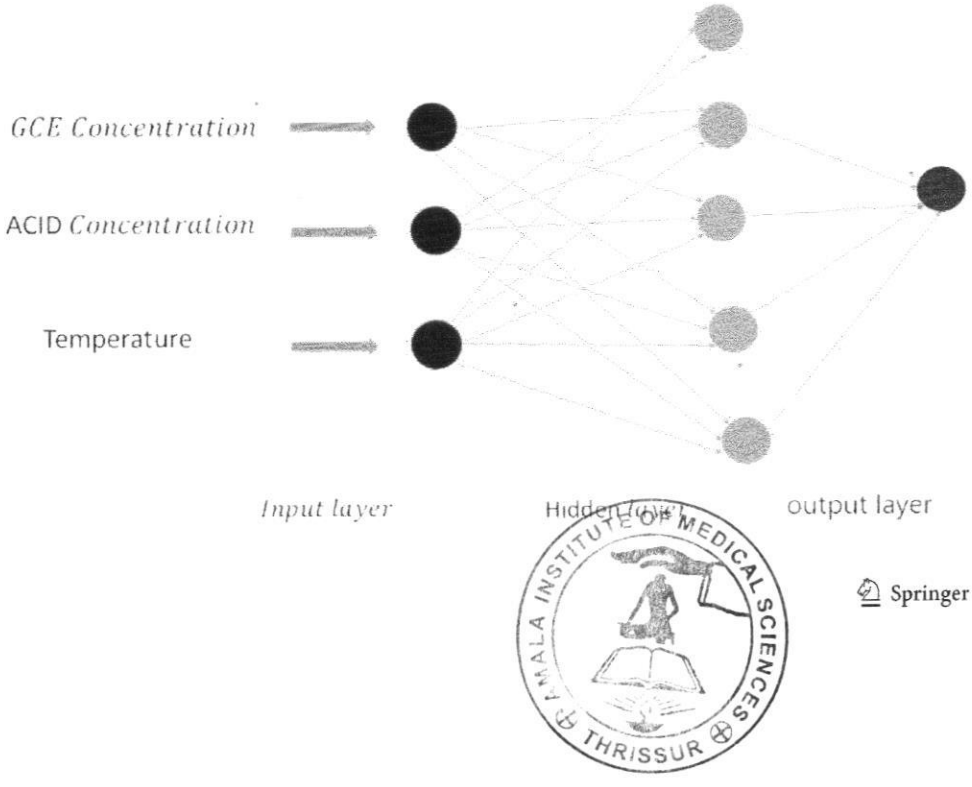

Table 1 Level of factors of BBD with coded and uncoded form

Sl. no	Factor	Code	Unit	Level of factors		
				Low (− 1)	Center (0)	High (1)
1	Temperature	X_1	K	313	323	333
2	GCE concentration	X_2	v/v%	1	3	5
3	Acid concentration	X_3	M	0.5	1	1.5

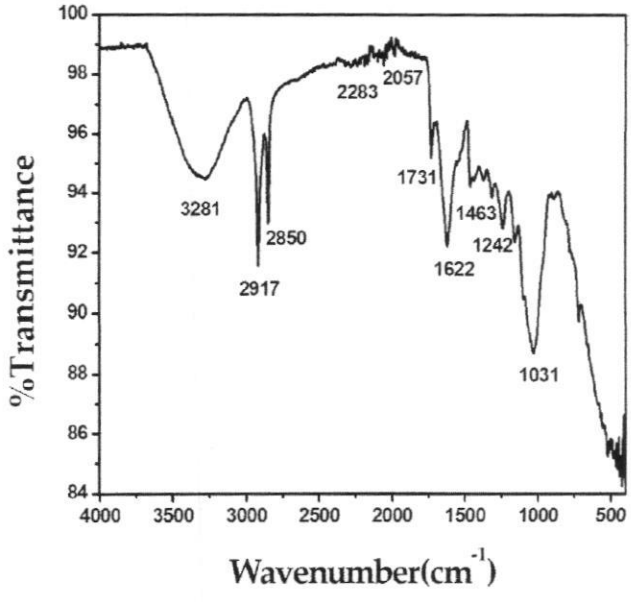

Fig. 5 FTIR spectrum of GCE

3 Results and Discussions

3.1 FTIR Spectroscopy

FTIR spectrum of GCE (Fig. 5) displays distinctive stretching and bending frequencies for different bonds. The O–H stretching vibration, a hydrogen bonding band, is indicated by the broad band at 3281 cm^{-1} Alkyl C–H stretching bonds are represented by two strong peaks at 2917 and 2850 cm^{-1}, whereas > C=O stretching band was seen at 1731 cm^{-1}. Carboxylic acids can be attributed to this peak. Aliphatic and aromatic C=C stretching vibrations are responsible for the peaks at 1622 and 1463 cm^{-1}, respectively. Weak bands of C–O stretching vibration were visible at 1242 and 1031 cm^{-1}. In summary, heteroatoms, aromatic rings, and unsaturated molecules are responsible for the distinct peaks of GCE. The hydroxyl groups present in the GCE molecules facilitate their adsorption onto the mild steel surface, forming a protective film. This adsorbed layer acts as a barrier, blocking corrosive species and thereby reducing the rate of corrosion.

Table 2 Weight loss measurements of mild steel with and without GCE in 1 M HCl and 0.5 M H_2SO_4 at room temperature for 24 h

Conc. (v/v %)	Corrosion rate (mm/yr)		Inhibition efficiency (η%)	
	1 M HCl	0.5 M H_2SO_4	1 M HCl	0.5 M H_2SO_4
Blank	3.95	35.57	–	–
1	1.77	18.83	55.12	47.06
2	1.44	16.92	63.49	52.41
3	1.20	15.08	69.53	57.59
4	1.08	13.22	72.48	62.82
5	0.32	8.70	91.73	75.53

3.2 Weight Loss Measurements

3.2.1 Effect of Concentration

Weight loss measurements were used to assess the stability of the adsorption layer on the metal surface. Table 2 showed the corrosion rate (υ) and inhibition efficiency (η%) in both acid media. Metal corrosion potency in 1 M HCl and 0.5 M H_2SO_4 solutions rose in synchrony with GCE content.

In 1 M HCl at room temperature, GCE showed an extreme η% value of 91.73% at the maximum concentration (5 v/v%) and a lower η% value of 55.12% at the lowest concentration (1 v/v%). GCE demonstrated marginally higher metal corrosion inhibition efficiency in hydrochloric acid medium compared to sulphuric acid medium. At 5 v/v%, the greatest η% in 0.5 M H_2SO_4 was 75.53%. The corrosion inhibition efficiency depends on surface coverage of inhibitor molecules. At higher GCE concentrations, more inhibitor molecules adsorb onto the metal surface which causes greater surface coverage and less acidic corrosion of mild steel. The anticorrosion activity of GCE, which is made up of several complex phytochemicals, can be linked to the electron-donating capabilities of the hydroxyl groups, carbonyl groups, heteroatoms, and unsaturated compounds that are present in GCE. Compared to the sulphate ions, the chloride ions had less hydration. As a result, chloride ions may adsorb differently than sulphate ions [25]. Since there are enough deposited Cl^- ions on the metal surface to provide negative charges towards the acidic media, hydroxycitric acid (HCA) adsorbs largely in its cationic form.

When compared with reported extracts, GCE demonstrates outstanding inhibition efficiency. Vibha Joshi et al., investigated that *Piper chaba* extract showed 86.53% anticorrosion performance at 1 g/L extract by coating for mild steel in 2 M H_2SO_4 [26]. Vishwajeet Bachhar and co-workers reported that *Calyptocarpus vialis* extract showed 82.69% corrosion inhibition efficiency for mild steel in 2 M H_2SO_4 by weight loss method [27]. Rajesh Haldhar et al., found *Quercus palustris* leaves extract as a green corrosion inhibitor for low-carbon steel having ~91% corrosion inhibition efficiency in acidic media at 1.00 g/L. GCE exhibited better IE (91.73%) in 1 M HCl than all these recently cited works [28].

3.2.2 Effect of Temperature

Weight loss data at four distinct temperatures (303, 313, 323, and 333 K) were used to assess the impact of temperature on metal corrosion process. Table 3 calculates the fluctuations in corrosion rate and inhibition efficiency, which are displayed in Fig. 6. The data clearly shows a direct relationship between temperature and corrosion rate. The inhibitory potency for 5% GCE concentration in HCl solution significantly decreased from 91.73 to 72.08% when the temperature was raised from 303 to 333 K. Similarly, at the maximum concentration investigated, the inhibitory potency dropped from 75.53 to 62.46% in H_2SO_4 medium. This pattern could be explained by GCE molecules desorbing off the metal surface at high temperatures, which disintegrates the protective layer of metal [29].

Table 3 Corrosion rate (υ) and inhibition efficiency (η%) of GCE in 1 M HCl and 0.5 M H_2SO_4 at different temperatures for 24 h

Medium	Conc (v/v%)	υ (303 K)	η% (303 K)	υ (313 K)	η% (313 K)	υ (323 K)	η% (323 K)	υ (333 K)	η% (333 K)
1 M HCl	Blank	3.95	–	13.11		22.05	–	31.77	–
	1	1.77	55.12	6.23	52.48	10.94	50.40	16.78	47.18
	2	1.44	63.49	5.72	56.37	10.09	54.25	15.56	51.02
	3	1.20	69.53	4.15	68.34	8.13	63.14	13.69	56.91
	4	1.08	72.48	3.79	71.09	8.05	63.50	13.28	58.20
	5	0.32	91.73	2.26	82.76	5.01	77.28	8.87	72.08
0.5 M H_2SO_4	Blank	35.57	–	58.27	–	86.25	–	106.2	–
	1	18.83	47.06	32.69	43.89	50.95	40.92	64.14	39.63
	2	16.92	52.41	28.58	50.95	45.58	47.15	59.64	43.87
	3	15.08	57.59	25.36	56.47	40.95	52.52	54.91	48.32
	4	13.22	62.82	22.98	60.56	36.23	57.99	51.92	51.13
	5	8.70	75.53	15.77	72.93	30.14	65.05	39.88	62.46

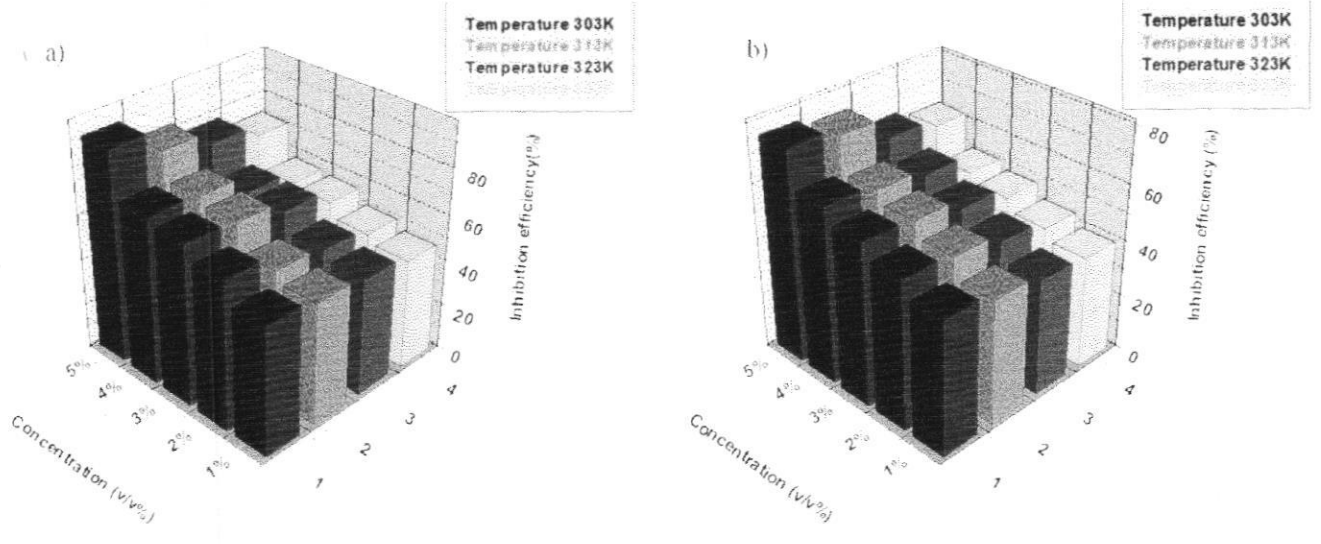

Fig. 6 Variation in inhibition efficiency of GCE in **a** 1 M HCl, **b** 0.5 M H_2SO_4 at elevated temperatures

Metal corrosion activation energy was determined using Arrhenius equation (Eq. (3)). For mild steel in acidic environments with and without GCE, plot of log K vs. 1/T is shown in Figs. 7a and 8a. From transition state theory, variables like entropy of activation (ΔS^*) and enthalpy of activation (ΔH^*) were derived. ΔH^* and ΔS^* values are represented by the slope and intercept of log K/T vs. 1/T plots (Figs. 7b and 8b). Table 4 shows that all thermodynamic parameters were computed, including pre-exponential factor (A) and activation energy (E_a). E_a values from Table 4 indicate that the metal corrosion activation energy is higher for the solution without GCE compared to that with GCE. Metal dissolution rate was found to decrease with increasing GCE concentration, due to corresponding increase in activation energy (E_a) [30]. Positive enthalpy of activation values demonstrated the endothermic nature of metal corrosion [31]. ΔH^* and ΔS^* readings rose in tandem with GCE concentration.

3.3 Adsorption Isotherm

Surface coverage and temperature were found to be inversely linked to one another based on weight loss measurements. This suggests that at higher temperatures, the corrosion products become less stable. Elevated temperatures have the potential to (1) accelerate the kinetic oxidation reaction and (2) accelerate the rate of desorption. At higher temperature, the metal surface's electrical charge raised which also suggesting that surface coverage and temperature have an inverse relationship.

The presence of active adsorption sites on the metal surface is blocked by the deposited inhibitor molecules. This could be because the inhibitor and the metal surface interact

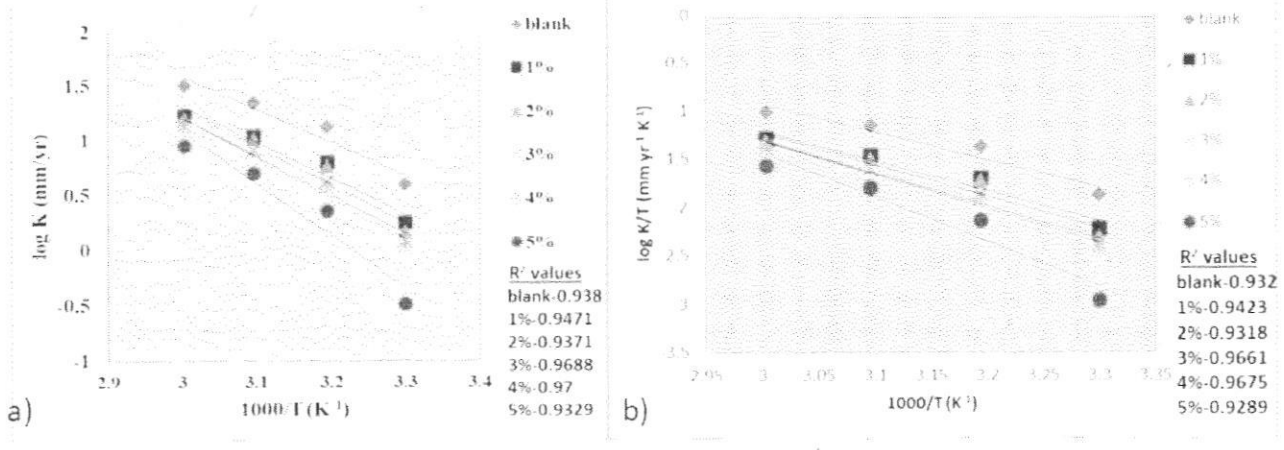

Fig. 7 Arrhenius plots of **a** log K vs 1000/T, **b** log K/T vs 1000/T with and without GCE in 1 M HCl

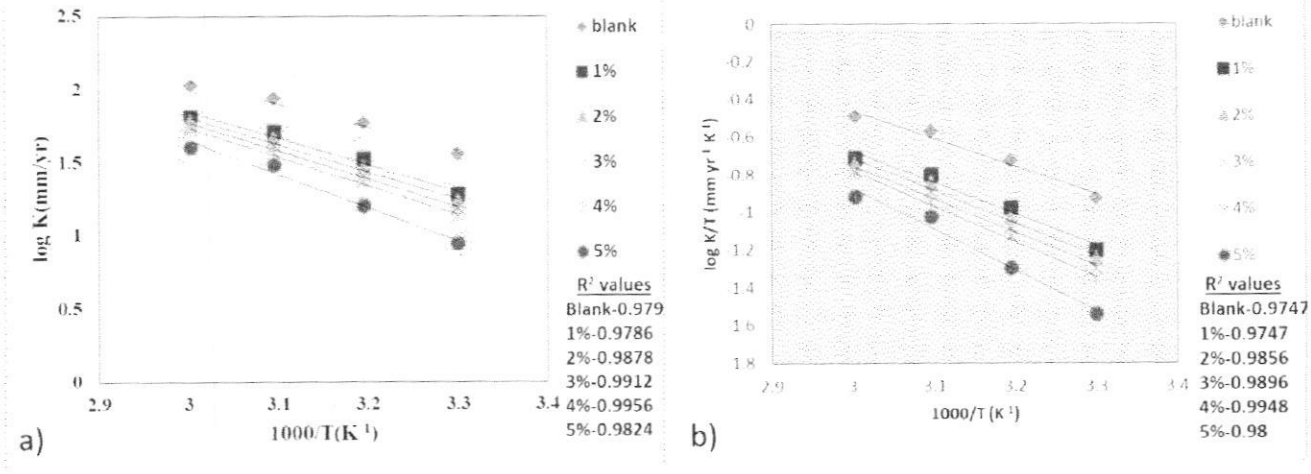

Fig. 8 Arrhenius plots of **a** log K vs 1000/T, **b** log K/T vs 1000/T with and without GCE in 0.5 M H_2SO_4

Table 4 Thermodynamic parameters of mild steel corrosion with and without GCE in 1 M HCl and 0.5 M H_2SO_4

Medium	Conc (v/v %)	E_a (kJ mol^{-1})	A	ΔH^* (kJ mol^{-1})	ΔS^* (J mol^{-1} K^{-1})
1 M HCl	Blank	57.24	3.58×10^{10}	54.60	−44.78
	1	61.70	9.40×10^{10}	59.06	−36.76
	2	65.09	3.03×10^{11}	62.45	−27.00
	3	67.18	5.42×10^{11}	64.54	−22.19
	4	69.67	1.31×10^{12}	67.03	−14.83
	5	90.45	1.79×10^{15}	87.81	45.17
0.5 M H_2SO_4	Blank	30.96	8.16×10^{6}	28.30	−114.51
	1	34.72	1.92×10^{7}	32.08	−107.36
	2	35.72	2.54×10^{7}	33.08	−105.07
	3	36.63	3.22×10^{7}	34.01	−103.09
	4	38.32	5.50×10^{7}	35.68	−98.630
	5	43.88	3.31×10^{8}	41.24	−83.710

more strongly than the metal surface and water molecules do. Adsorption model for metal-inhibitor interactions is typically determined using the Langmuir, Temkin, Freundlich, El-Awady, Flory–Huggins and Frumkin, isotherms [32]. Frumkin isotherm, which plots log [1/c(θ/(1 − θ))] vs. θ for 1 M HCl, was determined to have the best fit. On the other hand, Freundlich isotherm obeyed in 0.5 M H_2SO_4. Frumkin and Freundlich isotherms appropriate for the adsorption of GCE molecules on the metal surface in 1 M HCl and 0.5 M H_2SO_4 are displayed in Fig. 9a and b, respectively.

A noticeable departure of the slope from unity indicated that the isotherm could not be firmly applied, even though the linearity of the isotherm demonstrated that the adsorption of GCE obeyed the Freundlich isotherm in H_2SO_4. The apparent heterogeneity on the metal surface in sulphuric acid solution can be used to explain the slope's deviation from unity [33].

Mechanism of GCE adsorption on the metal surface can be inferred from the relationship between ΔG^0_{ads} and adsorption equilibrium constant K_{ads} [34], as illustrated in Eq. (9).

$$\Delta G^0_{ads} = -RT \ln \left(55.5\, K_{ads}\right) \tag{9}$$

The adsorption behaviour of GCE molecules on the mild steel surface was both physisorption and chemisorption, as demonstrated by ΔG^0_{ads} for GCE-mild steel adsorptions, which were − 26.98 and − 29.70 kJ mol^{-1} in 1 M HCl and 0.5 M H_2SO_4, respectively [35]. K_{ads} values in 1 M HCl and 0.5 M H_2SO_4 were determined to be 2572.016 and 867.227, respectively for GCE adsorption. GCE molecules preferentially adsorb onto the metal surface in HCl medium as opposed to H_2SO_4 media, according to higher values of K_{ads}.

Figure 10 shows the reliable surface interaction of the GCE molecules on mild steel. The primary components of GCE are mainly involved in corrosion inhibition, despite the presence of a myriad of other compounds. The strong adsorption of HCA and HCA lactone onto the metal

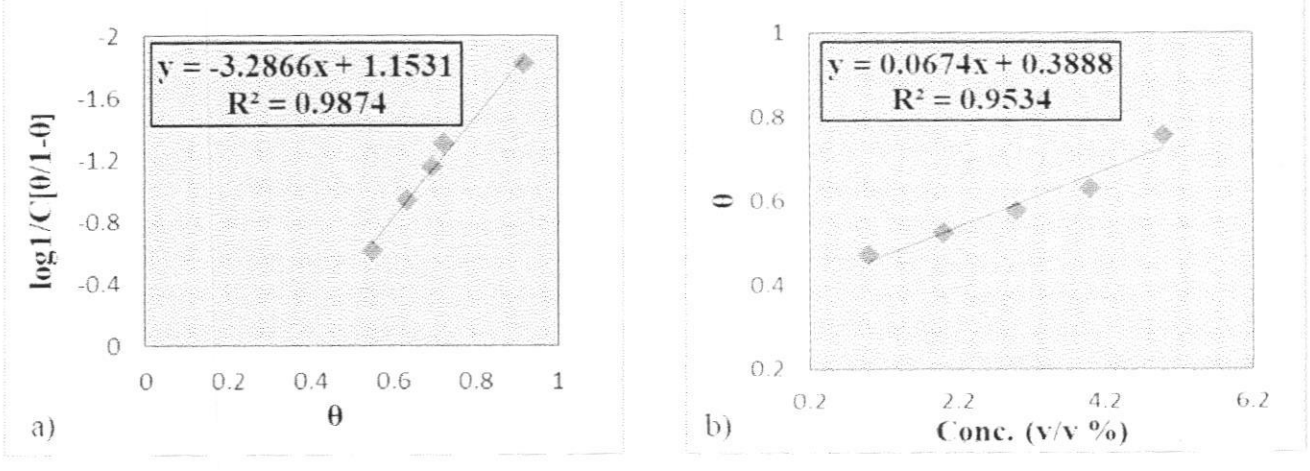

Fig. 9 **a** Frumkin adsorption isotherm of GCE on mild steel in 1 M HCl and **b** Freundlich isotherm of GCE on mild steel in 0.5 M H_2SO_4

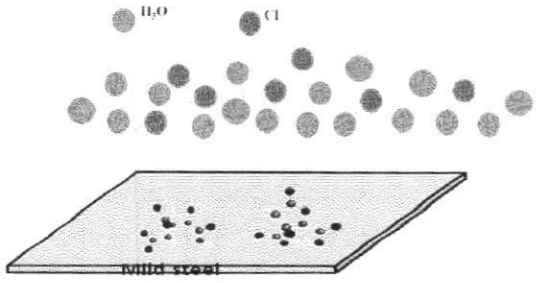

Fig. 10 Interaction diagram of GCE molecules with mild steel

surface occurred through electron donation from the oxygen atoms found in their alcoholic, acidic, and lactone functional groups. This leads to the development of a protective layer that inhibits metal corrosion. Additionally, HCA and HCA lactones may engage in back-donation interactions, in which d-electrons from the metal are transferred to the π^* orbitals of these molecules. Apart from these chemisorption interactions, physisorption of GCE also occurs. Initially, chloride or sulfate ions present in the acidic medium migrate toward the surface of mild steel and contribute to its cathodic activity. Subsequently, the larger cationic molecules of GCE were adsorbed onto the metal surface via a substitutional adsorption mechanism, replacing the smaller acid ions. This process disrupts both anodic and cathodic reactions associated with corrosion, ultimately reducing the rate of metal dissolution.

3.4 Electrochemical Impedance Spectroscopy

Mild steel corrosion impedance responses in 1 M HCl with and without GCE are shown in Fig. 11 and 0.5 M H_2SO_4 in Fig. 12, as Nyquist and Bode graphs respectively. Nyquist plot's depressed semicircular form indicates that a charge-transfer reaction occurs during the metal dissolving process [36]. An increase in the Nyquist plot's diameter with relation to concentration was used to calculate the ability of GCE molecules to slow down metal corrosion. Bode plots show that, in comparison to the blank experiment, the phase angle peaks grew wider and higher as the GCE concentration ascended. This was explained by mild steel's decreased capacitive behaviour, which showed how GCE molecules interacted with the metal surface [37]. The findings of impedance study are shown in Table 5. Using Eq. (3), the percentage inhibition efficiency was determined.

As shown in Table 5, R_{ct} values increased with rising GCE concentration, whereas C_{dl} values exhibited an opposite trend. The addition of GCE leads to an increase in R_{ct} values, indicating stronger inhibition efficiency. The decrease in C_{dl} values is attributed to the adsorption of GCE molecules, which displace water molecules at metal–solution interface. Mild steel surface develops an adsorption layer as a result, which lowers the rate of metal corrosion. Compared to sulphuric acid, GCE showed noticeably superior metal protection in hydrochloric acid. The maximum efficiency in sulphuric acid was only 72.06%, while the maximum efficiency in HCl was 89.73%. This outcome correlates with weight loss measurements.

3.5 Potentiodynamic Polarization Studies

Potentiodynamic polarisation studies have examined how mild steel anodic dissolution and cathodic hydrogen reduction vary with and without GCE because redox reactions control metal corrosion. Tafel and linear polarisation graphs

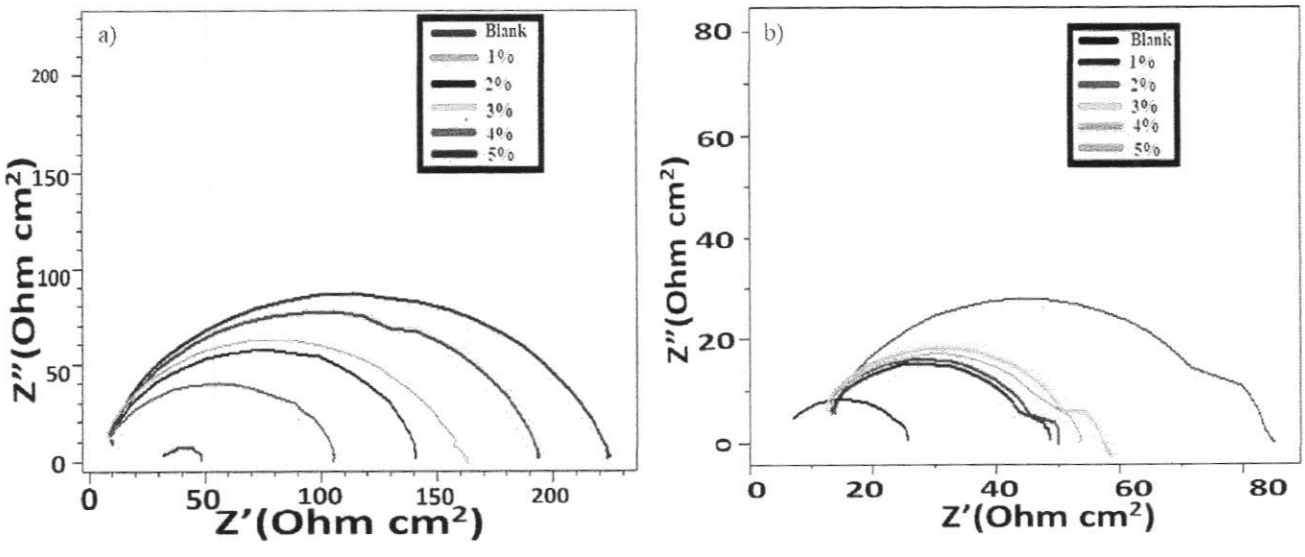

Fig. 11 Nyquist plots of mild steel with and without GCE in **a** 1 M HCl and **b** 0.5 M H_2SO_4

for mild steel at different GCE concentrations in 1 M HCl and 0.5 M H_2SO_4 are displayed in Figs. 13 and 14. Linear fragment of the anodic and cathodic Tafel plots was extrapolated using E_{corr} values to yield i_{corr} values. GCE significantly altered the slope of the curves at all concentrations, according to Tafel plots, suggesting that adding GCE to acid solutions regulated oxidation–reduction reactions.

This could limit cathodic hydrogen evolution processes and reduce mild steel's anodic dissolution [38]. Table 6 provides a summary of the potentiodynamic polarisation parameters obtained from Tafel and linear polarisation plots as well as the associated computed inhibition efficiencies. Table 6 shows that, when dipped in an acidic environment, the corrosion potential values shift from negative to more positive, going from uninhibited metal

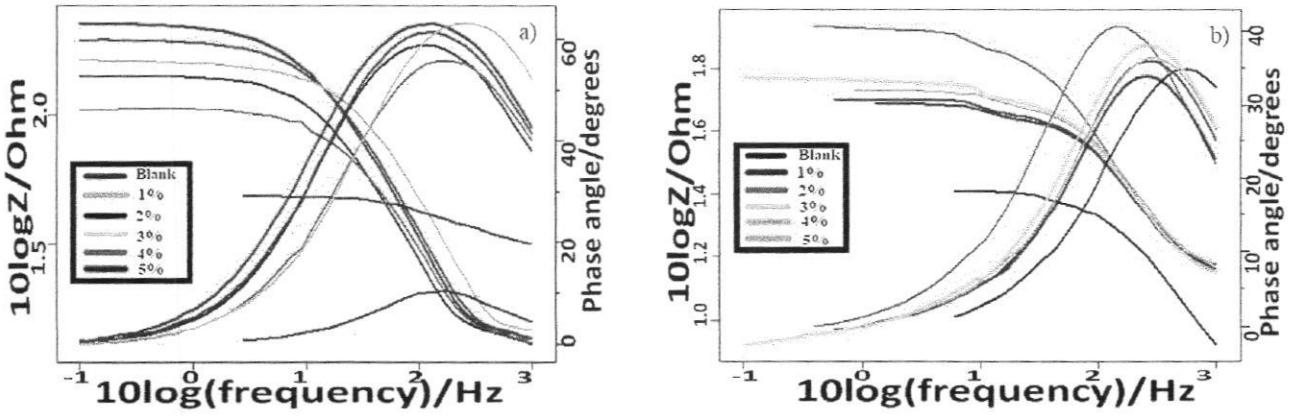

Fig. 12 Bode plots of mild steel with and without GCE in **a** 1 M HCl and **b** 0.5 M H_2SO_4

Table 5 Impedance parameters for mild steel in 1 M HCl and 0.5 M H_2SO_4 with and without GCE

Conc. (v/v %)	1 M HCl			0.5 M H_2SO_4		
	R_{ct} (Ωcm^2)	C_{dl} (μFcm^{-2})	η_{EIS}%	R_{ct} (Ωcm^2)	C_{dl} (μFcm^{-2})	η_{EIS}%
Blank	15.7	78.8	–	18.1	47.4	–
1	32.1	72.0	51.09	33.5	48.0	45.97
2	40.6	62.4	61.33	35.1	48.8	48.43
3	44.2	60.9	64.47	38.4	45.4	52.86
4	48.8	56.9	67.82	42.2	46.9	57.10
5	153	53.6	89.73	64.8	43.6	72.06

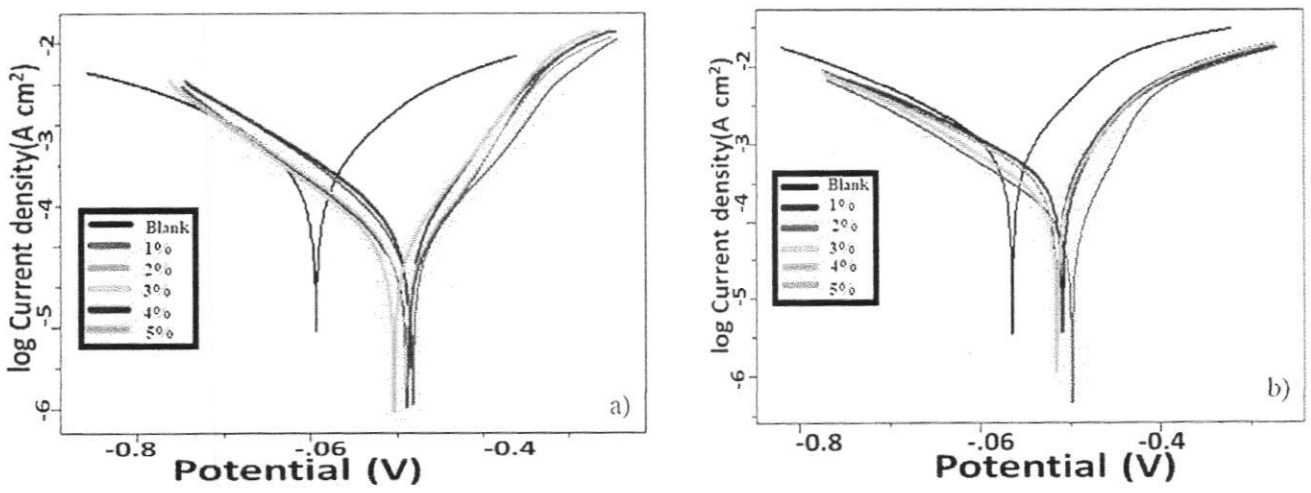

Fig. 13 Tafel plots of mild steel with and without GCE in **a** 1 M HCl and **b** 0.5 M H_2SO_4

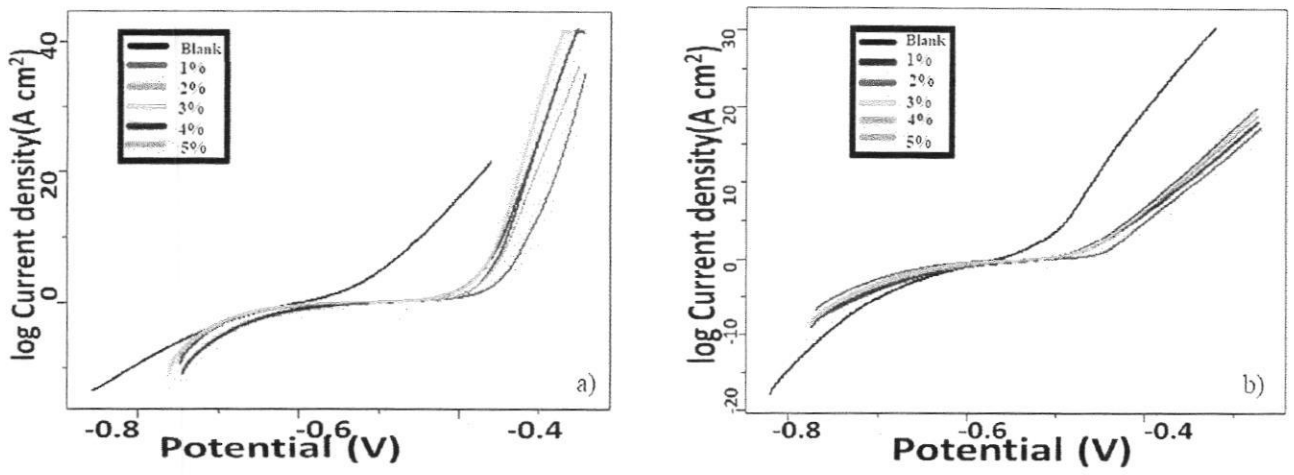

Fig. 14 Linear polarization plots of mild steel with and without GCE in **a** 1 M HCl and **b** 0.5 M H_2SO_4

to inhibited metal. Nevertheless, there has not been any specific analysis of this shift. It is possible to relate this to GCE's mixed manner of inhibition [39]. This pattern demonstrates how GCE molecules promote mild steel metal passivation by their contact with metal surface, successfully sealing the surface against further reaction. At higher concentrations, GCE exhibited strong inhibition efficiencies of 92.51% in 1 M HCl and 74.93% in 0.5 M H_2SO_4, resulting in a significant decrease in current density.

Polarization data indicated that the enhanced resistance of mild steel in acidic solutions containing GCE could be attributed to its strong corrosion inhibition properties. Polarisation resistance was 217.5 Ω cm^2 in 1 M HCl and 167.1 Ω cm^2 in 0.5 M H_2SO_4 at 5 v/v% GCE concentration. The increase in polarization resistance with higher GCE concentration suggests that complex compounds in the extract may prevent further polarization of mild steel at metal–acid interface [40].

3.6 Electrochemical Noise Measurements

It is simple to identify pitting corrosion on mild steel by looking for changes in the electrode potential. Figure 15 displays the current noise data for mild steel in 1 M HCl and 0.5 M H_2SO_4 solutions with different GCE concentrations. As the concentration of GCE increased, amplitude of current noise dropped, suggesting that the corrosion process was significantly stopped. Figure 16 displays PSD graphs for metal dipped in 1 M HCl and 0.5 M H_2SO_4 with different GCE concentrations. This demonstrates that current noise's magnitude reduces with increasing frequency. It is clear from looking at the aforementioned figure that in

Table 6 Potentiodynamic polarization parameters for mild steel in 1 M HCl and 0.5 M H_2SO_4 with and without GCE

	Tafel data						Polarization data	
Medium	Conc. (v/v %)	$-E_{corr}$ (mV)	i_{corr} (μAcm^2)	b_a (mV/dec)	$-b_c$ (mV/dec)	η_{pol}%	R_p (Ω)	η_{Rp}%
1 M HCl	Blank	597.9	1240	166	221	–	33.14	–
	1	492.2	441	97	172	64.43	68.92	51.91
	2	506.2	424	94	139	65.80	82.73	59.94
	3	507.3	378	104	157	69.51	84.99	61.00
	4	487.3	358	89	166	71.12	89.21	62.85
	5	495.3	92.8	72	132	92.51	217.5	84.76
0.5 M H_2SO_4	Blank	602.2	1616	184	193	–	25.30	–
	1	567.9	792	194	179	50.99	57.16	55.73
	2	574.7	743	186	174	54.02	60.06	57.87
	3	572.5	726	187	180	55.07	62.44	59.48
	4	581.6	567	176	152	64.91	82.82	69.45
	5	577.9	405	167	144	74.93	167.1	84.85

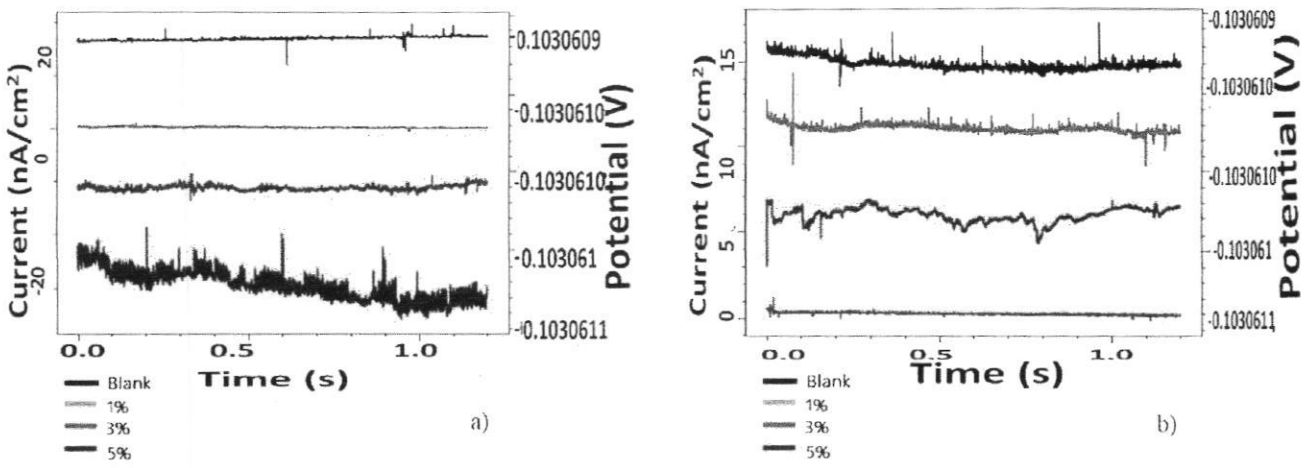

Fig. 15 Current noise plots for mild steel with and without GCE in **a** 1 M HCl, **b** 0.5 M H_2SO_4

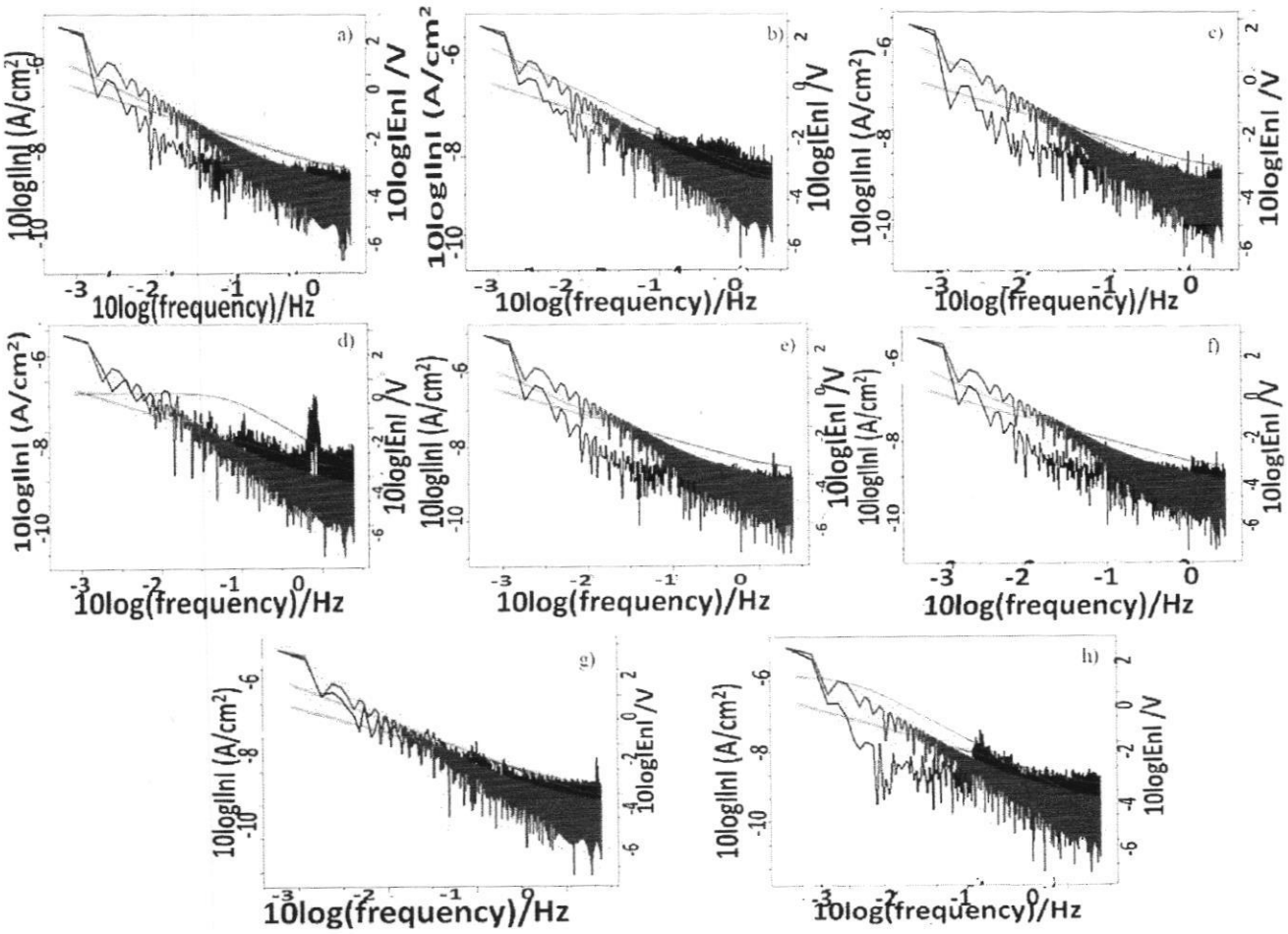

Fig. 16 Power spectral density plots of mild steel in 1 M HCl **a** without GCE, **b** 1% GCE, **c** 3% GCE, **d** 5% GCE; Power spectral density plots of mild steel in 0.5 M H_2SO_4, **e** without GCE, **f** 1% GCE, **g** 3% GCE, and **h** 5% GCE

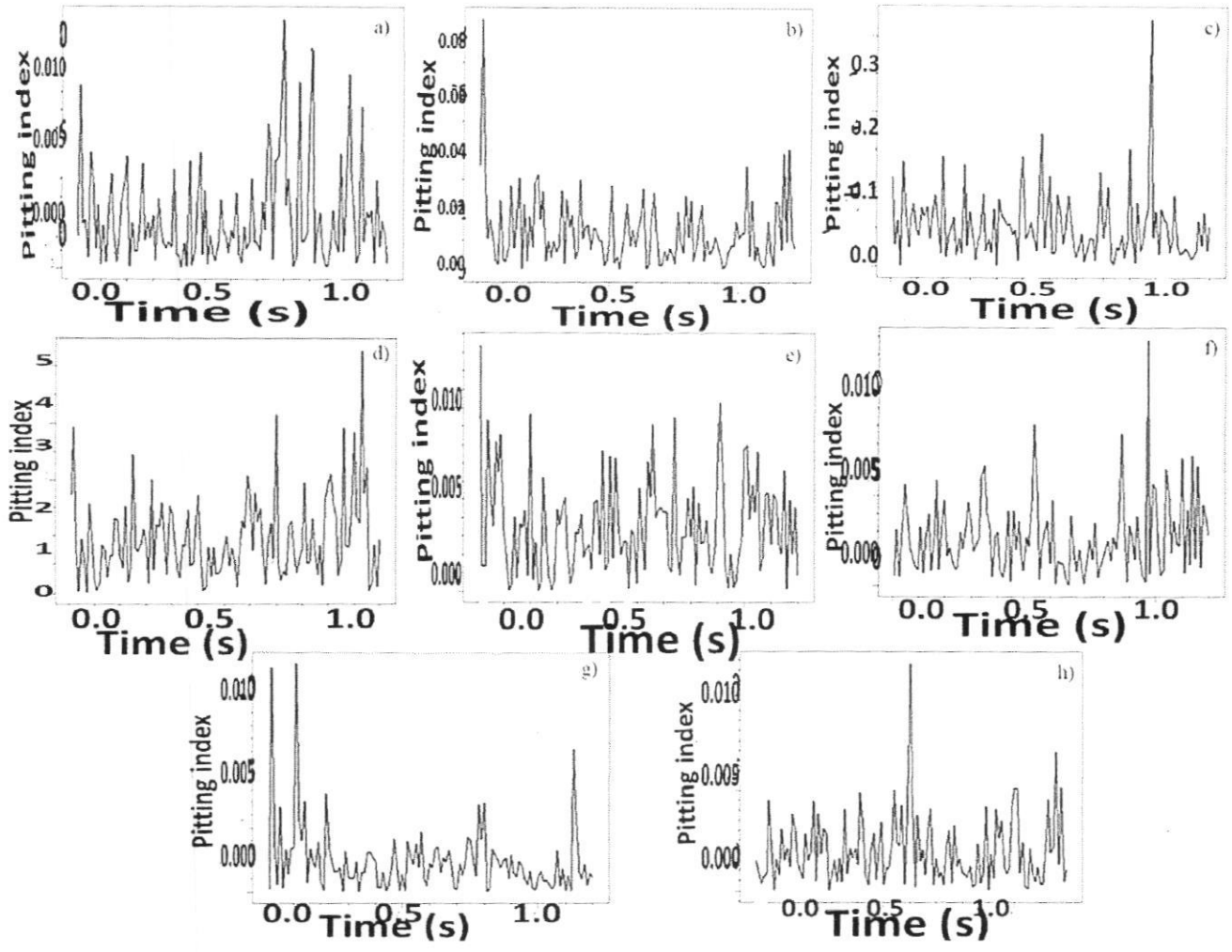

Fig. 17 Pitting index curves of mild steel in 1 M HCl **a** without GCE, **b** 1% GCE, **c** 3% GCE, **d** 5% GCE; Pitting index curves of mild steel in 0.5 M H_2SO_4, **e** without GCE, **f** 1% GCE, **g** 3% GCE, and **h** 5% GCE

both acid solutions, current noise for uninhibited metal was higher than that for inhibited metal [41]. Ability of GCE molecules to prevent metal corrosion in acidic environments was examined.

It is also known as pitting resistance equivalent number (PREN), or pitting index. It is a sign of how resistant a metal is to corrosion [42]. Pitting index curves are displayed in Fig. 17 for mild steel exposed to acid solutions with and without different concentrations of GCE.

It is evident from the figure that pitting index value improved in parallel with GCE concentration. At the highest concentration under investigation, pitting index value was higher in HCl media, while it was lower in H_2SO_4 medium. It can be inferred from a comparison of the pitting index values for inhibited and blank metal that the metal with GCE exhibits superior corrosion resistance in aggressive conditions. Additionally, it demonstrated that GCE had better anti-corrosion properties in 1 M HCl than in 0.5 M H_2SO_4.

3.7 Atomic Force Microscopy

Due to its effectiveness as a tool for surface morphological research, AFM analysis supports the surface interaction of GCE on mild steel. Figure 18a–e displays three-dimensional images of AFM analysis of metal over 24-h period of immersion. Table 7 lists the parameters for surface roughness. Surface topography of smoothed metal surface is depicted in Fig. 18a, where its average roughness value (R_a) is 26.11 nm lower than that of the metal dipped in acid media. Figure 18b and d represents the corroded metal surfaces exposed to 1 M HCl and 0.5 M H_2SO_4, respectively. R_a values for the blank experiment were higher than those of the metal dipped in acid solutions containing 5 v/v% GCE. Figure 18c and e display the inhibited metal surfaces in 1 M HCl and 0.5 M H_2SO_4, respectively. R_a values of the inhibited metal fell between those of the smoothened metal and the metal from blank experiment. This suggests that mild steel generated a

protective adsorption coating of GCE molecules, preserving smooth and fine metal surfaces [43]. Additionally, it was noted that the metal with GCE had lower roughness characteristics in 1 M HCl than in 0.5 M H_2SO_4. This provides more evidence that GCE has a stronger inhibitory capability in HCl than in H_2SO_4.

3.8 Quantum Mechanical Calculations

A major factor in determining an inhibitor's capability is its electronic and spatial molecular structures. The optimised geometry, HOMO, and LUMO of two crucial GCE components, HCA, and HCA lactone, are displayed in Fig. 19. The following quantum mechanical parameters are calculated and provided in Table 8: HOMO (E_{HOMO}) and LUMO (E_{LUMO}) energies, chemical potential (μ), ionisation energy (I), electron affinity (A), electronegativity (χ), hardness (η), and the number of electrons transferred (ΔN) of HCA and HCA lactone.

Enhanced inhibitory potential was facilitated by lower ionization energy values and reduced energy gap (ΔE). As shown in Table 8, HCA lactone primarily reduces the energy gap (ΔE) and increases the likelihood of electron donation, evidenced by its lower ΔE value compared to HCA. Additionally, HCA contributes to the improved inhibitory efficiency of GCE. The distribution of electrons in a molecule is measured by electronic chemical potential (μ). Large values of μ are generally thought to promote the adsorption of an inhibitor, even though the electronic chemical potential (μ) cannot predict the direction of corrosion inhibition [44]. The increased μ values for HCA and HCA lactone suggest that these two important components work well together to provide inhibitory efficacy of GCE. A higher ΔN value indicates that the inhibitor molecule donates a greater number of electrons to the vacant d-orbitals of the metal surface, resulting in stronger adsorption and enhanced corrosion inhibition efficiency.

3.9 Artificial Neural Networks (ANNs)

The total experimental samples of the ANN model were split into three categories: training data (70.77%), validation data (11.11%), and testing data (11.11%) for the prediction of IE in the H_2SO_4 media. For the HCl media, 68.88% of the data were utilised for training, 15.55% for validation, and 15.55% for testing. (Table 9).

Table 10 provides a description of the experimental and ANN output values of inhibition efficiency (IE). R values were close to 1, and the MSE values were comparatively low, indicating that the model was effectively trained [45]. As the ANN model was trained using experimental IE. To determine IE of H_2SO_4 ANN model utilized 4 neurons whereas HCl model used 5 neurons. One hidden layer was used in each case. Justification of ANN architecture with number hidden layers and neurons has been described in the Fig. 20 a and b respectively.

Figures 21 and 22 show the comparison of training, validation, and testing values for the prediction of IE in acidic media. The R-values were closer to 1. Thus, the experimental IE and ANN model values were strongly correlated.

ANN training phase error histogram for IE prediction in the two distinct acidic media is displayed in Figs. 23 and 24. It is evident from the numbers that the majority of errors are located close to the yellow line, which represents the zero-error threshold. The error levels of the three distinct experimental samples used for testing, validation, and training were explained by the histogram. Additionally, the statistics show that a low error rate was achieved throughout the training phase.

3.10 Statistical Analysis

3.10.1 Optimization of Factors for Inhibition Efficiency (IE%)

Corrosion inhibition potential was significantly impacted by temperature, GCE concentration, and acid concentration, according to weight loss measurements. They were chosen as independent factors in this study as a result. Tables 11 and 12, respectively, display Box-Bahnken design (BBD) structure and three levels based on the design of test variables (X_1, X_2, and X_3) for HCl and H_2SO_4. Fifteen experimental runs were carried out. There was a direct correlation between concentration of GCE and corrosion inhibition efficiency. At 313 K, this technique achieved high inhibitory efficiency with 5 v/v% GCE concentration in 0.5 M HCl and H_2SO_4. Excellent efficiency was obtained for appropriate combination of three components employed in the current investigation by using RSM. Quadratic Eqs. (10) and (11) for HCl and H_2SO_4 respectively indicate the regression model that was created for the relationship between test components (X_1, X_2, and X_3) and inhibition efficiency.

$$IE = 670 - 3.32X_1 + 27.55X_2 - 99.7X_3 + 0.00436X_1^2 + 0.013X_2^2 - 2.09X_3^2 - 0.0673X_1X_2 + 0.2833X_1X_3 + 0.841X_2X_3 \quad (10)$$

$$IE = 461 - 2.12X_1 + 4.44X_2 - 90.4X_3 + 0.00255X_1^2 + 0.349X_2^2 + 3.29X_3^2 - 0.0028X_1X_2 + 0.2337X_1X_3 + 0.287X_2X_3 \quad (11)$$

where IE represents the inhibition efficiency, X_1 denotes the temperature, X_2 denotes the GCE concentration, and X_3 denotes the acid concentration.

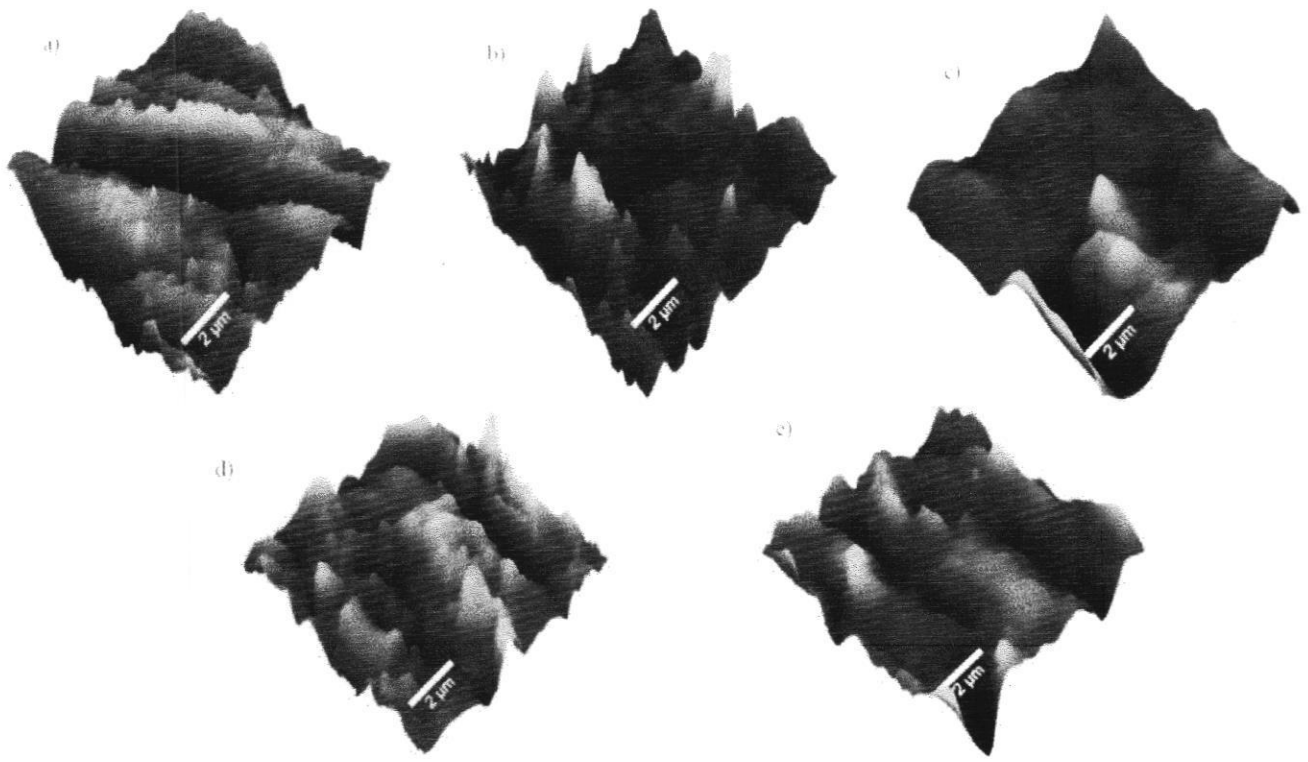

Fig. 18 Topography of mild steel surface **a** smoothened, **b** in 1 M HCl, **c** in 1 M HCl with 5 v/v% GCE, **d** in 0.5 M H_2SO_4, and **e** in 0.5 M H_2SO_4 with 5 v/v% GCE

Table 7 Surface roughness parameters of mild steel by AFM analysis

Sample	R_{pp} (nm)	R_q (nm)	R_a (nm)
Smoothened mild steel	205.27	32.92	26.11
Mild steel in 1 M HCl	965.86	79.50	55.07
Mild steel in 1 M HCl with 5 v/v% GCE	727.45	58.27	36.46
Mild steel in 0.5 M H_2SO_4	2176.62	231.72	180.48
Mild steel in 0.5 M H_2SO_4 with 5 v/v% GCE	1026.18	120.38	86.46

A regression model was used to create analysis of variance (ANOVA) [46]. Tables 13 and 14, respectively, show ANOVA results for HCl and H_2SO_4 at 95% significance level. The most important value in this table that establishes if a factor is significant is the P-value. 0.05 was chosen as the degree of essentialness (α). A careful examination of the table reveals that linear and square terms of GCE concentration had a P-value below 0.05, while linear and two-way interaction terms in HCl had a P-value below 0.05. This clarifies why the most important terms are temperature, acid concentration, and GCE concentration. According to Pareto charts (Fig. 25), the most notable influence on inhibition efficiency in both acidic media is the linear term GCE concentration. R^2 and R^2(adj) values' proximity to unity indicates a model that fits the experimental data better [47]. For HCl, R^2 and R^2(adj) values were 0.9983 and 0.9954, while for H_2SO_4, they were 0.9962 and 0.9895. The predicted model's best fit to the experimental data is evident from these values. As a result, this approach allows for rapid evaluation of the outcomes.

Regression analysis was supported by the main effect charts. This demonstrates how the parameters under test affected the response [48]. The main effect graphs for the fitted means of inhibitory efficiency in HCl and H_2SO_4 media are displayed in Fig. 26. The highest inhibitory efficiency was obtained with 5 v/v% concentration of GCE at an operating temperature of 313 K with 0.5 M concentrations of HCl and H_2SO_4, according to the analysis of the preceding figure. Velocity of bombardment between the molecules increases as the temperature rises because the kinetic energy of inhibitor molecules rises as well. This inclination tendency may reduce inhibition efficiency by hindering the inhibitors' ability to form an adsorbed protective layer on the metal surface. When concentration of

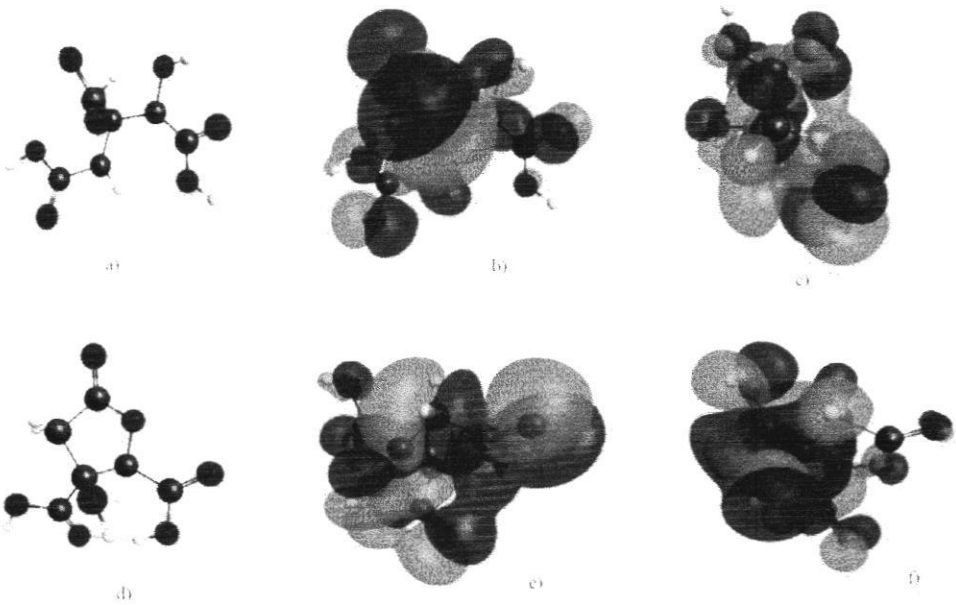

Fig. 19 **a** Optimized geometry, **b** HOMO, and **c** LUMO of HCA, **d** Optimized geometry, **e** HOMO, and **f** LUMO of HCA lactone

Table 8 Quantum mechanical parameters (in eV) of HCA (I) and HCA lactone (II)

Molecule	E_{HOMO}	E_{LUMO}	ΔE	I	A	μ	X	η	ΔN
I	−2.131	0.090	2.22	2.13	−0.09	−1.02	1.02	1.11	2.692
II	−2.148	0.066	2.21	2.14	−0.06	−1.04	1.04	1.10	2.691

Table 9 Data distribution of the ANN Model for the prediction of IE

H_2SO_4	Samples	MSE	R
Training	35	0.964131	0.9947
Validation	5	0.119651	0.9996
Testing	5	0.475075	0.9982
HCl			
Training	31	0.588951	0.9974
Validation	7	0.741728	0.9991
Testing	7	0.323147	0.9787

acid increased, a similar finding was made. At the same time, adding 1 to 5 v/v% GCE increased the GCE's inhibitory capacity. Because of the adsorption of inhibitor molecules, the corrosion rate dropped and efficiency enhanced when the inhibitor was present.

Interaction plot for the two acids, which interprets any factor interaction, is displayed in Fig. 27. A substantial interaction between the components is indicated by any crossed lines in the interaction plot. Straight or parallel lines suggest that the components do not interact. The interaction plot for inhibitory efficiency for both acids showed no crossed lines, indicating that two-way interaction terms were unnecessary (Fig. 27). Temperature and acid concentration in HCl and H_2SO_4 showed imperfect parallel lines, indicating some interactions. These findings were also added to an ANOVA analysis.

Figures 28 and 29 [49] present contour and 3D surface plots that demonstrate the interrelationship among the examined variables affecting inhibition efficiency (IE%). The inhibition efficiency increased significantly when the GCE concentration was increased at a particular temperature. In contrast, the inhibition efficiency decreased as the temperature increased, which can be ascribed to the physisorption of GCE molecules on metal surface. The inverse relationship between inhibition efficiency and acid concentration strongly supports the corrosion of mild steel at 1.5 M HCl/H_2SO_4.

3.10.2 Response Optimization

Maximum IE was obtained using quadratic Eqs. (10) and (11) by optimising three tested parameters (temperature, GCE concentration, and acid concentration). This method is called, the desirability function method. The optimum conditions showed from response optimisation plots (Fig. 30) were 313 K, 5 v/v% concentration of GCE, and 0.5 M HCl/H_2SO_4 concentration and the resulting IE% were 87.62% and 68.69% in HCl and H_2SO_4 acids, respectively.

Table 10 Experimental and ANN output values for IE in HCl and H_2SO_4 media

GCE Conc (v/v%)	H_2SO_4 Conc (M)	Temp (K)	H_2SO_4 IE(%)	H_2SO_4 ANN IE(%)	HCl IE(%)	HCl ANN IE(%)
1	1	313	39.60	39.9982	52.48	51.1362
2	1	313	44.78	46.0342	56.37	58.1753
3	1	313	51.41	50.0803	68.34	68.8490
4	1	313	56.29	55.6420	71.09	72.0050
5	1	313	62.23	63.5878	82.76	82.6564
1	1	323	36.77	38.0411	50.40	48.7399
2	1	323	43.76	42.9958	54.25	55.0508
3	1	323	47.32	47.3019	63.14	63.2819
4	1	323	52.12	52.7534	63.50	64.5974
5	1	323	60.74	60.3846	77.28	77.2487
1	1	333	35.83	35.7349	47.18	46.7816
2	1	333	39.57	39.9691	51.02	52.3756
3	1	333	45.25	46.0741	56.91	58.6596
4	1	333	50.47	51.2619	58.20	57.6096
5	1	333	58.23	58.3426	72.08	72.2310
1	0.5	313	43.90	44.1872	56.73	56.3506
2	0.5	313	50.95	50.2230	65.16	64.4058
3	0.5	313	56.48	55.5052	74.27	74.2439
4	0.5	313	60.56	62.6564	78.32	79.6230
5	0.5	313	72.94	71.3729	83.48	84.4926
1	0.5	323	40.93	41.4392	54.79	53.8873
2	0.5	323	47.15	47.9918	62.94	60.1441
3	0.5	323	52.52	52.5792	68.38	67.5865
4	0.5	323	57.99	58.0447	70.64	73.2427
5	0.5	323	65.06	65.2324	79.43	79.3637
1	0.5	333	39.64	39.1662	50.80	51.5105
2	0.5	333	43.87	43.6600	57.19	56.4891
3	0.5	333	48.32	48.0772	62.66	61.8778
4	0.5	333	51.14	53.0440	67.70	67.3058
5	0.5	333	62.47	60.4200	75.13	75.4077
1	1.5	313	36.15	35.4734	46.61	46.1140
2	1.5	313	40.58	41.5982	53.52	52.2759
3	1.5	313	46.14	46.4441	60.61	60.5091
4	1.5	313	53.28	52.7719	67.94	68.0480
5	1.5	313	60.78	61.1368	78.11	77.3670
1	1.5	323	33.45	33.1896	44.22	43.9097
2	1.5	323	37.73	38.5758	50.11	50.2785
3	1.5	323	45.90	44.2455	58.54	57.4205
4	1.5	323	50.13	49.8211	62.70	62.7839
5	1.5	323	58.73	57.4035	72.22	71.5874
1	1.5	333	31.70	32.4695	40.36	41.3742
2	1.5	333	35.37	35.6812	48.83	47.6354
3	1.5	333	42.66	42.2863	54.66	53.6438
4	1.5	333	47.54	47.3086	56.34	57.0017
5	1.5	333	53.04	54.0091	63.62	64.2909

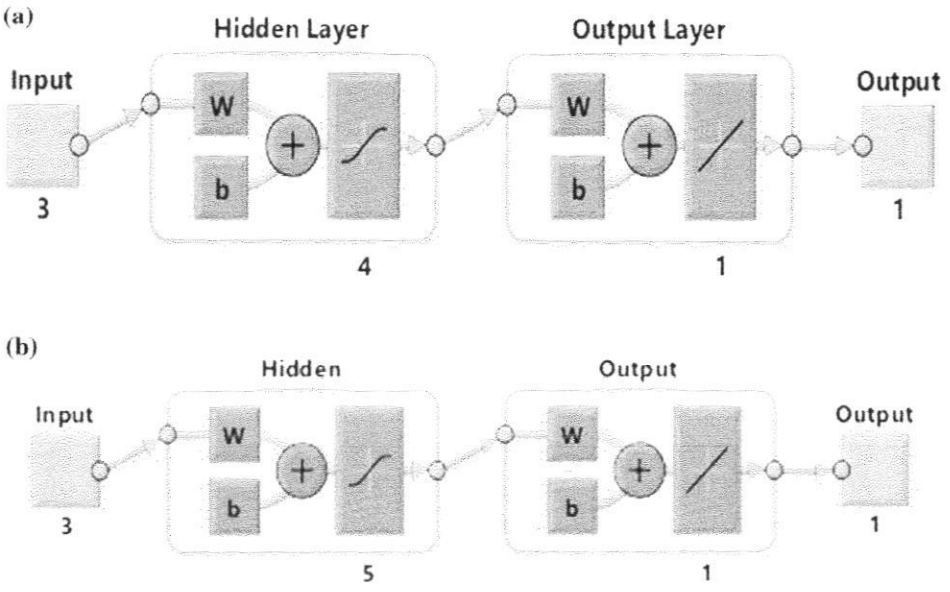

Fig. 20 **a** ANN architecture for IE in H_2SO_4 medium. **b** ANN architecture for IE in HCl medium

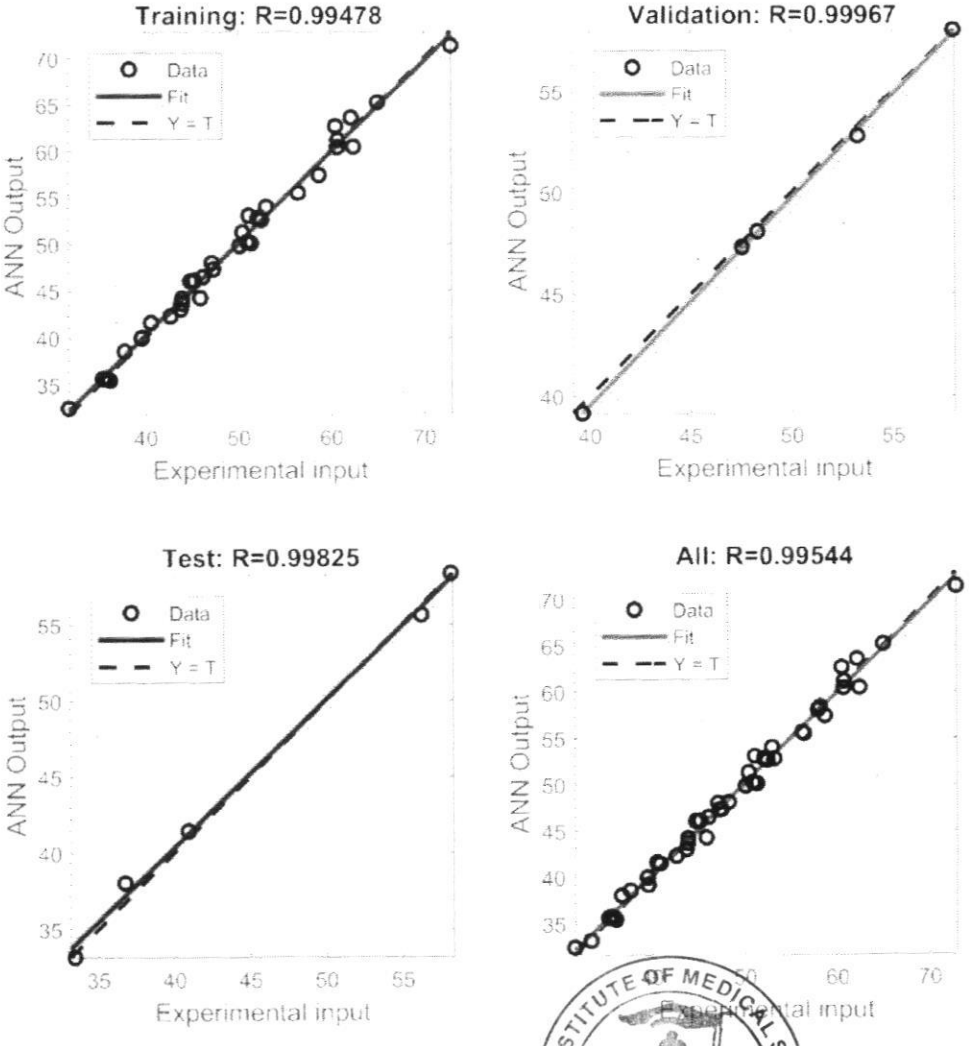

Fig. 21 ANN and experimental model on IE in H_2SO_4

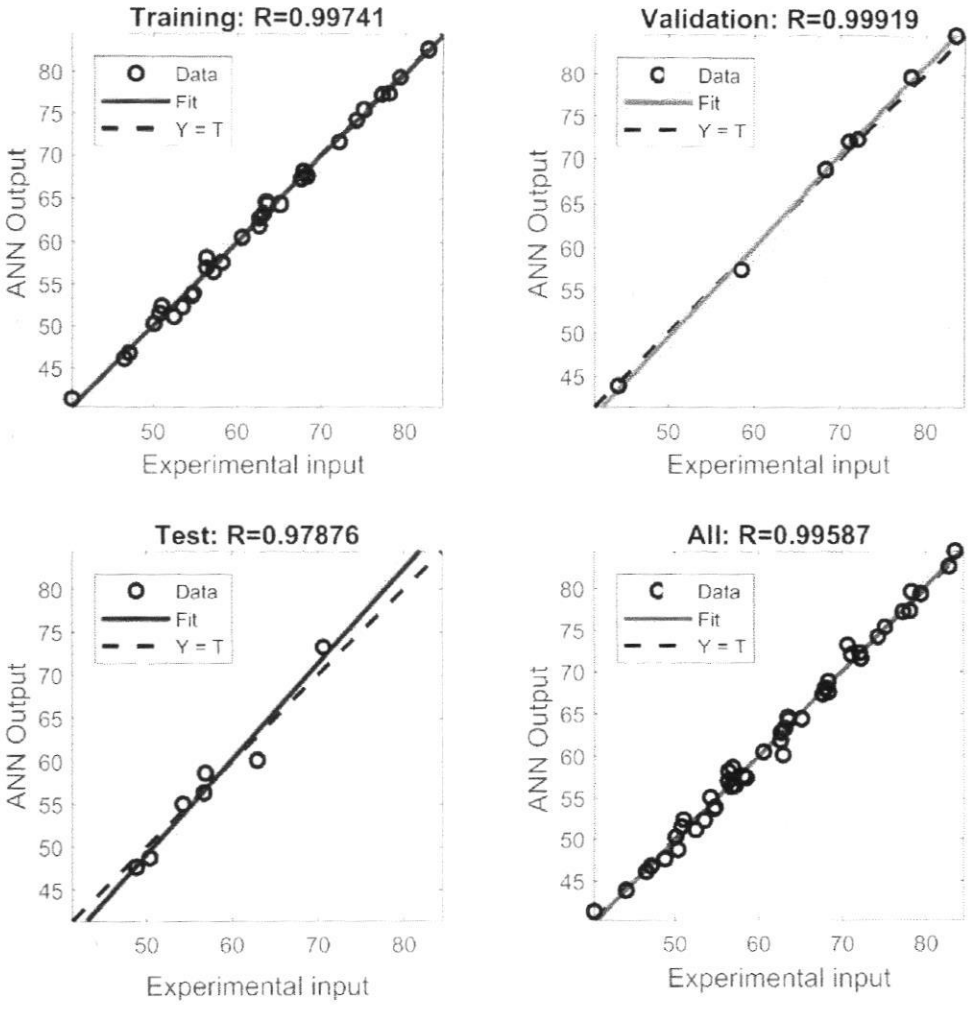

Fig. 22 ANN and experimental model on IE in HCl

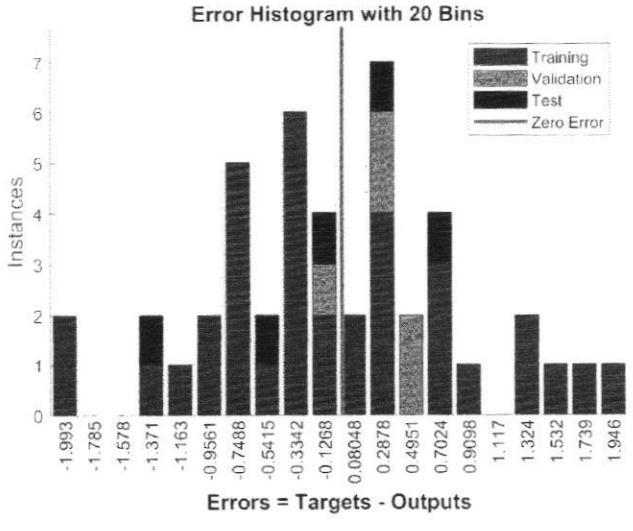

Fig. 23 Error histogram for the prediction of IE in H_2SO_4 medium

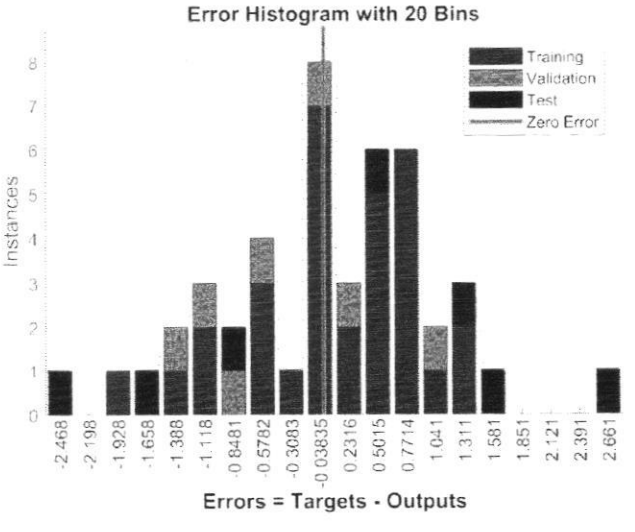

Fig. 24 Error histogram for the prediction of IE in HCl medium

Table 11 Experimental and predicted IE% from weight loss measurements and BBD for HCl medium

Run order	Actual level of factors			IE%		Residual
	X_1	X_2	X_3	Experimental	Predicted	
1	313	1	1	52.48	53.00	2.348
2	333	1	1	47.18	47.30	0.886
3	313	5	1	82.76	82.64	0.886
4	333	5	1	72.08	71.56	2.348
5	313	3	0.5	74.27	73.59	0.282
6	333	3	0.5	62.66	62.37	2.952
7	313	3	1.5	60.61	60.90	2.952
8	333	3	1.5	54.66	55.35	0.282
9	323	1	0.5	54.79	54.96	2.066
10	323	5	0.5	79.43	80.23	0.603
11	323	1	1.5	44.22	43.42	0.603
12	323	5	1.5	72.22	72.05	2.066
13	323	3	1	63.14	63.14	0.001
14	323	3	1	63.14	63.14	0.001
15	323	3	1	63.14	63.14	0.001

Table 12 Experimental and predicted IE% from weight loss measurements and BBD for H_2SO_4 medium

Run order	Actual level of factors			IE%		Residual
	X_1	X_2	X_3	Experimental	Predicted	
1	313	1	1	39.60	39.53	0.062
2	333	1	1	35.82	34.80	1.028
3	313	5	1	62.23	63.26	−1.028
4	333	5	1	58.23	58.29	−0.062
5	313	3	0.5	56.47	55.71	0.758
6	333	3	0.5	48.32	48.53	−0.207
7	313	3	1.5	46.13	45.92	0.207
8	333	3	1.5	42.65	43.41	−0.758
9	323	1	0.5	40.92	41.74	−0.821
10	323	5	0.5	65.05	64.78	0.269
11	323	1	1.5	33.45	33.72	−0.269
12	323	5	1.5	58.72	57.90	0.821
13	323	3	1	47.32	47.32	0
14	323	3	1	47.32	47.32	0
15	323	3	1	47.32	47.32	0

4 Conclusions

This study highlights the potential of *Garcinia cambogia* extract (GCE) as a green, eco-friendly corrosion inhibitor for mild steel in both 1 M HCl and 0.5 M H_2SO_4 environments. GCE demonstrated high inhibition efficiencies of 91.73 and 75.53% in 1 M HCl and 0.5 M H_2SO_4 respectively, at room temperature, analysed through weight loss, electrochemical (EIS, PDP), and surface analysis (AFM) techniques. The mixed-type inhibition behaviour, increased charge transfer resistance, and reduced double-layer capacitance suggest strong adsorption of GCE molecules on the mild steel surface. Quantum chemical calculations of its key components (HCA and HCA lactone) further validated for its inhibitory action.

Novelty lies in the use of a naturally occurring, sustainable and biodegradable extract that shows strong anti-corrosion performance in both acidic media, supported by a combination of experimental and computational methods, including RSM and ANN modelling for predictive efficiency.

However, limitations include reduced corrosion inhibition performance at elevated temperatures and the complex composition of plant extracts, which may vary between sources and batches.

Table 13 Analysis of variance for IE% in HCl medium

Source	DF	Adj SS	Adj MS	F-Value	P-Value
Model	9	1807.96	200.88	335.49	0.000
Linear	3	1788.01	596.00	995.35	0.000
Temperature	1	140.67	140.67	234.92	0.000
GCE Conc	1	1452.89	1452.89	2426.37	0.000
Acid Conc	1	194.46	194.46	324.76	0.000
Square	3	1.86	0.62	1.04	0.452
Temperature*Temperature	1	0.70	0.70	1.17	0.328
GCE Conc.*GCE Conc	1	0.01	0.01	0.02	0.906
Acid Conc.*Acid Conc	1	1.01	1.01	1.68	0.251
2-Way Interaction	3	18.09	6.03	10.07	0.015
Temperature*GCE Conc	1	7.24	7.24	12.09	0.018
Temperature*Acid Conc	1	8.02	8.02	13.40	0.015
GCE Conc.*Acid Conc	1	2.83	2.83	4.72	0.082
Error	5	2.99	0.60		
Lack-of-Fit	3	2.99	1.00	*	*
Pure Error	2	0.00	0.00		
Total	14	1810.96			

DF degrees of freedom, *Adj SS* adjusted sum of squares, *Adj MS* adjusted mean of squares, *F* Fischer's F-test value, *P* probability

Table 14 Analysis of variance for IE% in H_2SO_4 medium

Source	DF	Adj SS	Adj MS	F-Value	P-Value
Model	9	1287.93	143.10	147.40	0.000
Linear	3	1273.00	424.33	437.08	0.000
Temperature	1	47.06	47.06	48.47	0.001
GCE Conc	1	1114.86	1114.86	1148.34	0.000
Acid Conc	1	111.08	111.08	114.42	0.000
Square	3	9.13	3.04	3.13	0.125
Temperature*Temperature	1	0.24	0.24	0.25	0.640
GCE Conc.*GCE Conc	1	7.20	7.20	7.41	0.042
Acid Conc.*Acid Conc	1	2.49	2.49	2.57	0.170
2-Way Interaction	3	5.80	1.93	1.99	0.234
Temperature*GCE Conc	1	0.01	0.01	0.01	0.913
Temperature*Acid Conc	1	5.46	5.46	5.63	0.064
GCE Conc.*Acid Conc	1	0.33	0.33	0.34	0.586
Error	5	4.85	0.97		
Lack-of-Fit	3	4.85	1.62	*	*
Pure Error	2	0.00	0.00		
Total	14	1292.78			

DF degrees of freedom, *Adj SS* adjusted sum of squares, *Adj MS* adjusted mean of squares, *F* Fischer's F-test value, *P* probability

Future work should focus on isolating the most active compounds within GCE, exploring long-term stability under dynamic industrial conditions, and scaling up for practical application.

The industrial world highly recommends the development of environmentally sustainable corrosion inhibitors for solving both material and financial losses. In this research work, a green corrosion inhibitor- *Garcinia cambogia* extract (GCE)—is employed for mild steel in 1 M HCl and 0.5 M H_2SO_4 media.

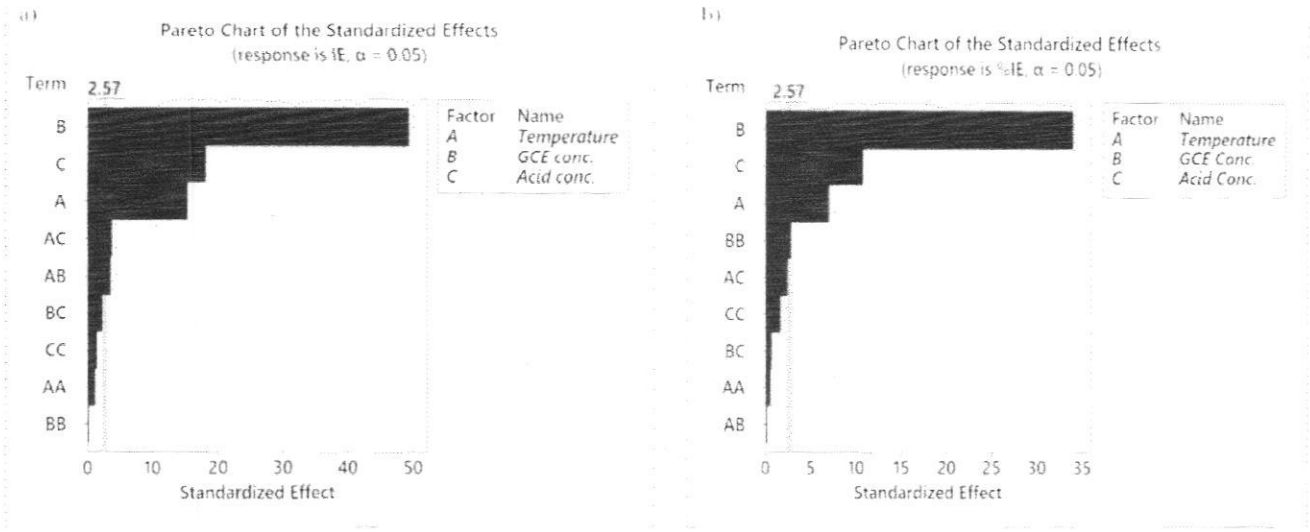

Fig. 25 Pareto chart of the standardized effects for IE% in **a** HCl, **b** H_2SO_4 medium

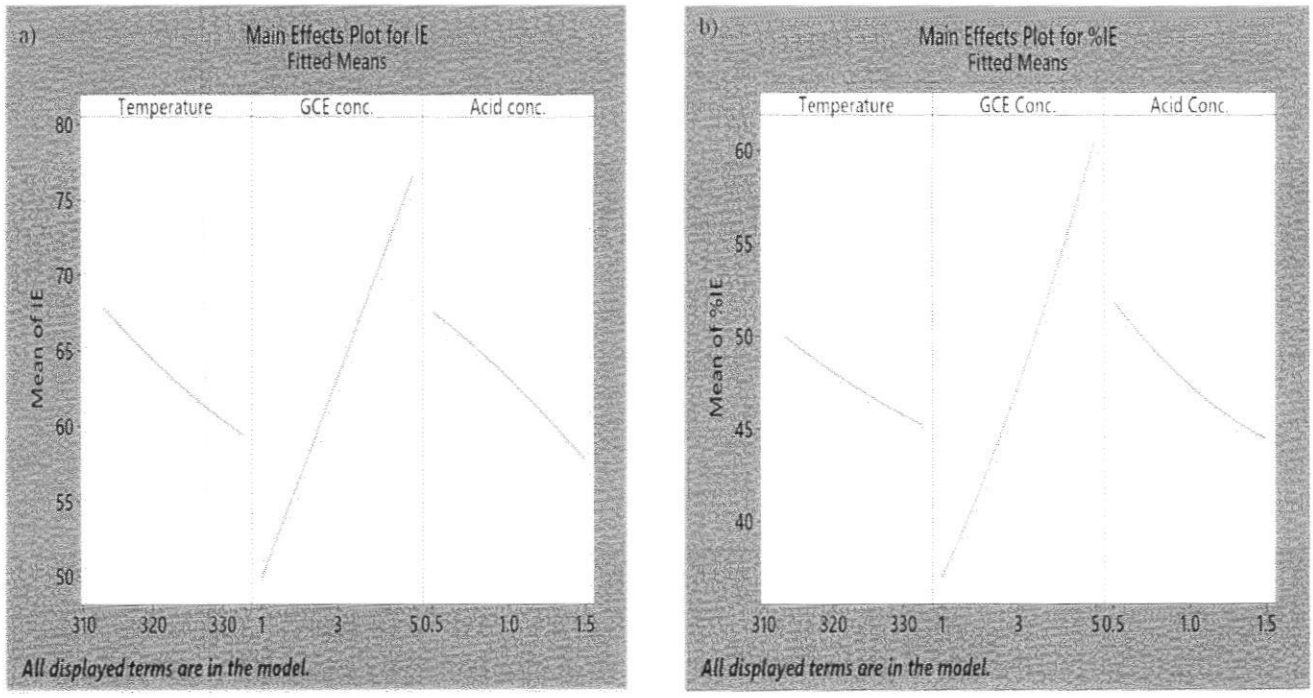

Fig. 26 Main effects plots for inhibition efficiency for mild steel in **a** HCl, **b** H_2SO_4 medium

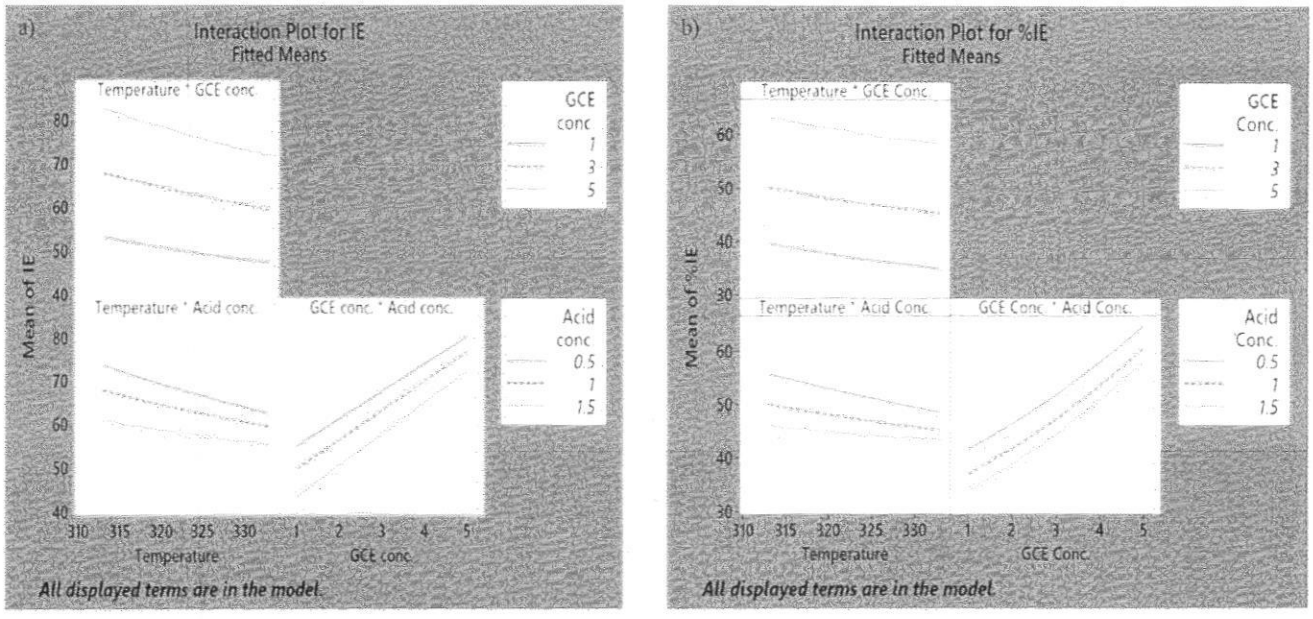

Fig. 27 Interaction plot for IE% in **a** HCl, **b** H_2SO_4 medium

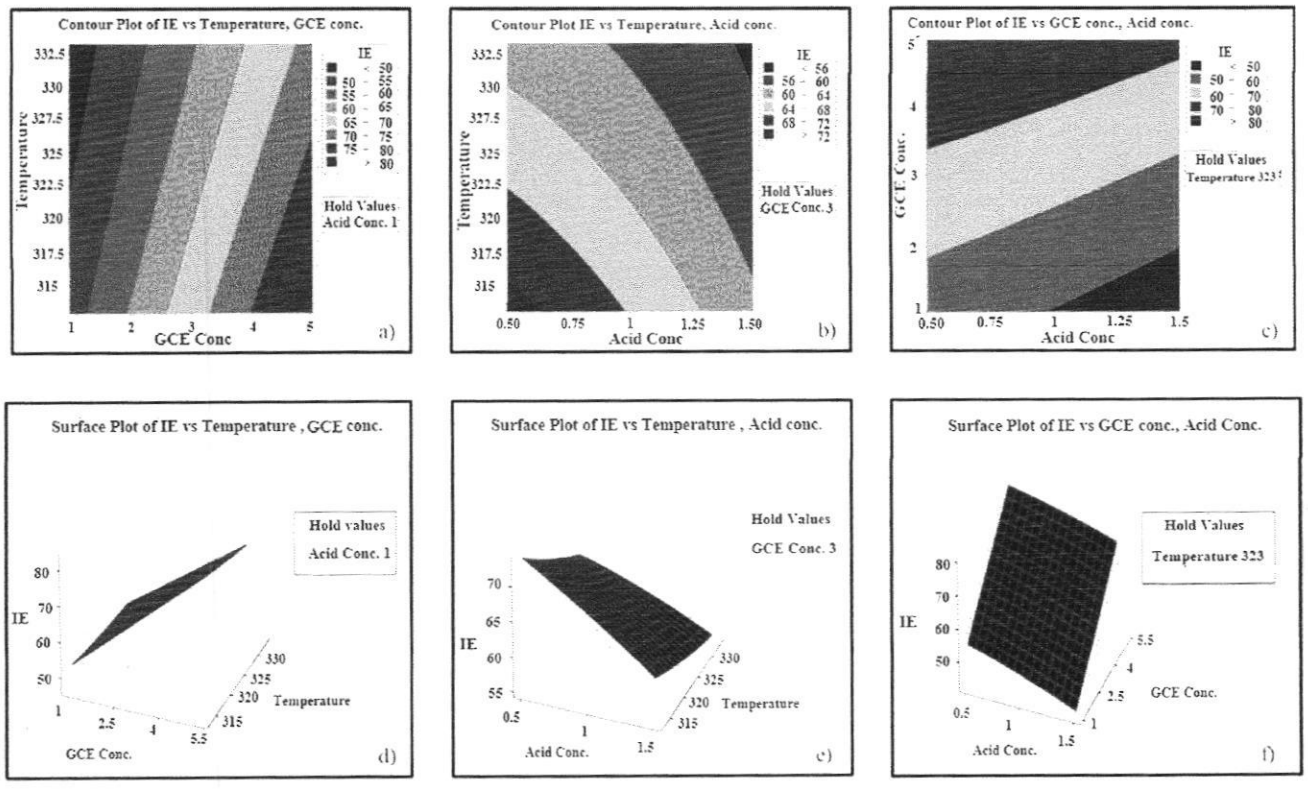

Fig. 28 Contours (**a**–**c**) and 3-D surface plots (**d**–**f**) for IE% in HCl

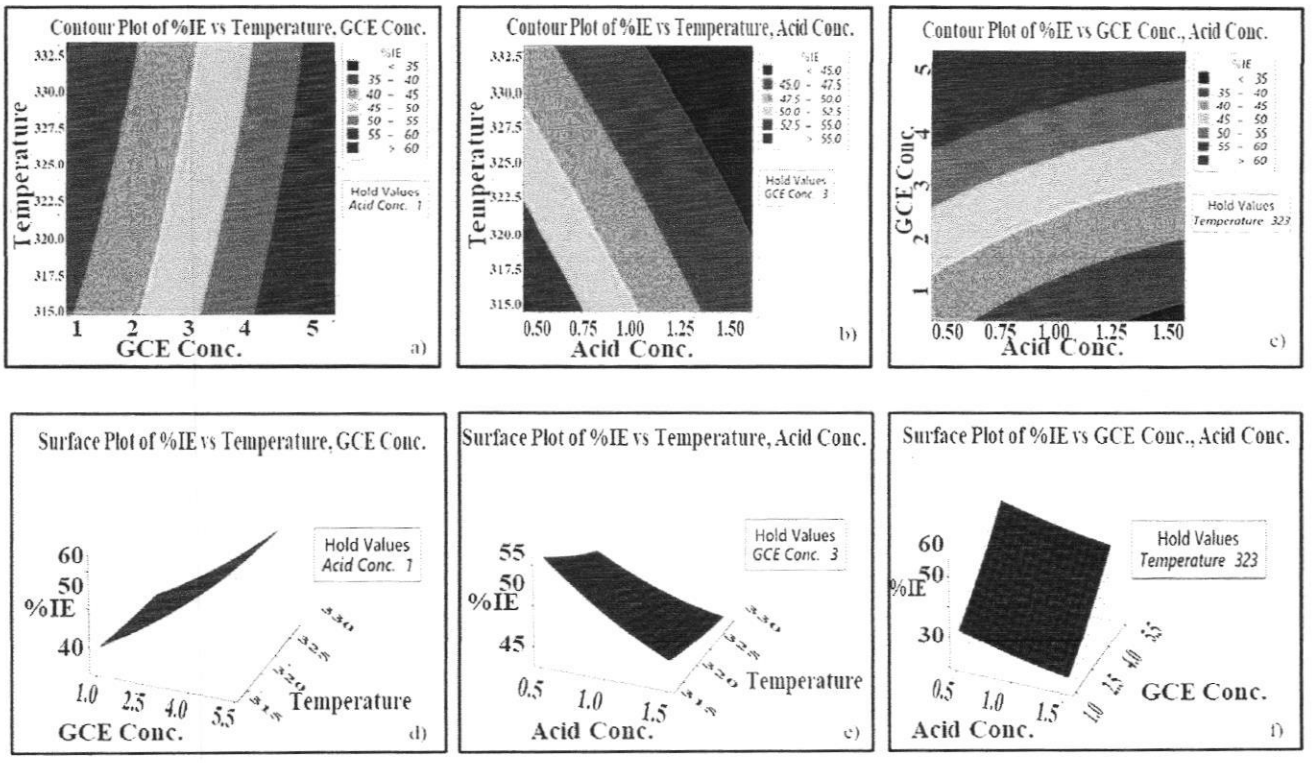

Fig. 29 Contours (**a**–**c**) and 3-D surface plots (**d**–**f**) for IE% in H_2SO_4

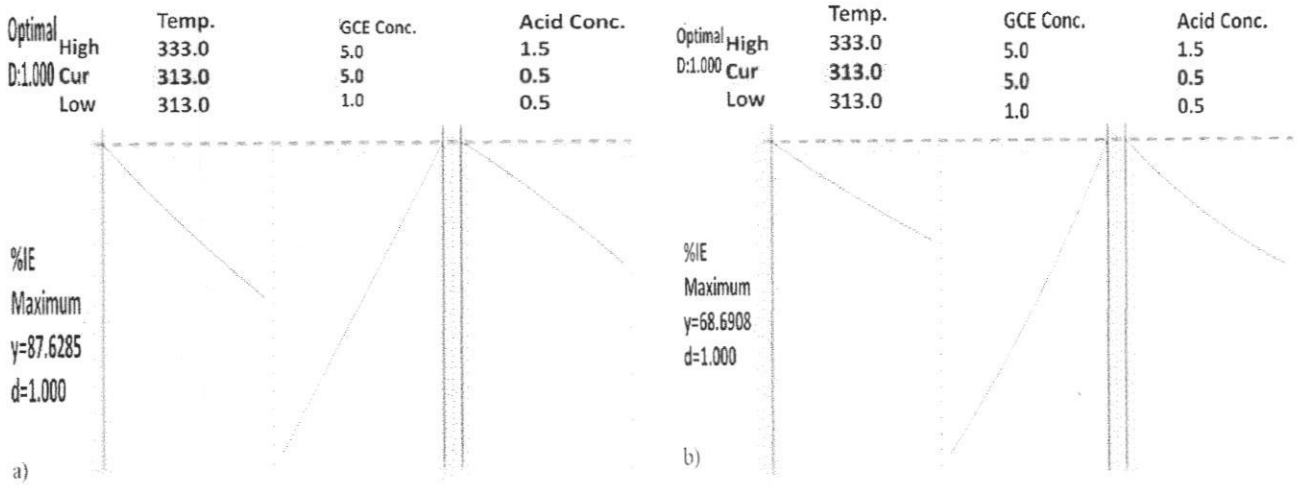

Fig. 30 Response optimization plot for IE% in **a** HCl, **b** H_2SO_4 medium

Author Contributions V.T, A.S. S.V, and R.J wrote the manuscript text. J.T. edited the manuscript draft. V.T and A.S did the RSM & ANN part. All authors reviewed the manuscript.

Funding Not applicable.

Data Availability No datasets were generated or analysed during the current study.

Declarations

Competing interests The authors declare no competing interests.

Ethical Approval Not applicable.

Clinical Trial Number Not applicable.

References

1. Mathew ZP, Rajan K, Augustine C, Joseph B, John S (2020) Corrosion inhibition of mild steel using poly (2-ethyl -2-oxazoline) in 0.1M HCl solution. Heliyon 6:e05560. https://doi.org/10.1016/j.heliyon.2020.e05560
2. Pêgas M, Fernández T, Magalhães M, Schöntag T, Lago D, Senna L, D'Elia E (2012) Inhibitory action of aqueous garlic peel extract on the corrosion of carbon steel in HCl solution. Corros Sci 65:360–366. https://doi.org/10.1016/j.corsci.2012.08.038
3. Sajadi GS, Naghizade R, Zeidabadinejad L, Golshani Z, Amiri M, Ali Hosseini SM (2022) Experimental and theoretical investigation of mild steel corrosion control in acidic solution by *Ranunculus arvensis* and *Glycine max* extracts as novel green inhibitors. Heliyon 8:e10983. https://doi.org/10.1016/j.heliyon.2022.e10983
4. Zaher A, Aslam R, Lee H-S, Khafouri A, Boufellous M, Alrashdi AA, El aoufir Y, Lgaz H, Ouhssine M (2022) A combined computational & electrochemical exploration of the Ammi visnaga L. extract as a green corrosion inhibitor for carbon steel in HCl solution. Arab J Chem 15:103573
5. Shainy K, Anupama K, Joseph A (2016) Excellent anticorrosion behavior of *Ruta graveolens* extract (RGE) for mild steel in hydrochloric acid : electro analytical studies on the effect of time, temperature, and inhibitor concentration. J Bio- Tribo-Corros 2:1–10. https://doi.org/10.1007/s40735-016-0032-5
6. Saxena A, Prasad D, Thakur KK, Kaur J (2020) PDP, EIS, and surface studies of the low-carbon steel by the extract of Tinospora cordifolia: a green approach to the corrosion inhibition. Arab J Sci Eng. https://doi.org/10.1007/s13369-020-04894-9
7. Saxena A, Thakur KK, Saxena KK, Chambyal S, Sharma A (2019) Electrochemical studies and surface examination of low carbon steel by applying the extract of Terminalia chebula. Mater Today Proc 26:1360–1367. https://doi.org/10.1016/j.matpr.2020.02.276
8. Amodu OS, Karabo Obed Ntwampe SKO, Odunlami M, Akintola JT, Akoro S (2019) Exploring *Musa paradisiaca* peel extract as a green corrosion inhibitor for mild steel using factorial design method. A. Singh (Ed.). IntechOpen, Rijeka. https://doi.org/10.5772/intechopen.82617
9. Oyewole O, Oshin T, Atotuoma BO (2021) *Corchorus olitorius* stem as corrosion inhibitor on mild steel in sulphuric acid. Heliyon 7:e06840. https://doi.org/10.1016/j.heliyon.2021.e06840
10. Ansari A, Ou-Ani O, Oucheikh L, Youssefi Y, Chebabe D, Oubair A, Znini M (2021) Experimental, theoretical modeling and optimization of inhibitive action of *Ocimum basilicum* essential oil as green corrosion inhibitor for C38 steel in 0.5 M H_2SO_4 medium. Chem Africa. https://doi.org/10.1007/s42250-021-00289-x
11. Ahmed J et al (2024) Evaluation of the corrosion inhibition potential of *Azadirachta indica* leaves on thermo mechanically treated steel rebars using an artificial neural network, electrochemical and spectroscopic approach. Cogent Eng. 11:2392208. https://doi.org/10.1080/23311916.2024.2392208
12. Krishnanjana K, Ganesh GM (2025) Green corrosion inhibition of *Punica granatum* peel powder on TMT in salt medium: outlooks from experiments and artificial neural networks. Green Chem Lett Rev 18:2525117. https://doi.org/10.1080/17518253.2025.2525117
13. Rameshkumar KB (2016) Diversity of Garcinia species in the Western Ghats: phytochemical perspective. https://doi.org/10.25173/978-81-924674-5-0
14. Joshi V, Bachhar V, Bhatia A, Rom T, Duseja M, Shukla RK (2025) Green synthesis of multifunctional AgFe nanoparticles using *Piper chaba* extract: evaluation of antioxidant, antidiabetic, and antibacterial activities. Colloids Surf A Physicochem Eng Asp 725:137619. https://doi.org/10.1016/j.colsurfa.2025.137619
15. Bachhar V, Joshi V, Bhatia A, Rom T, Duseja M, Shukla RK (2025) Green synthesis of AgFe bimetallic nanoparticles from *Calyptocarpus vialis* plant extract for enhanced catalytic reduction of 4-NP, antioxidant and antibacterial activities. J Environ Chem Eng 13:116829. https://doi.org/10.1016/j.jece.2025.116829
16. Joshi V, Bachhar V, Negi A, Mishra SS, Duseja M (2025) Green synthesis of silver nanoparticles using *Pachygone laurifolia* extract and pharmacological evaluation for antioxidant, antidiabetic, and antibacterial activity. J Mol Struct 1342:142730. https://doi.org/10.1016/j.molstruc.2025.142730
17. Binsi MP, Joby TK, Ragi K, Sini VC, Reeja J (2020) Interaction of two heterocyclic schiff bases derived from 2-acetyl pyridine on mild steel in hydrochloric acid: physicochemical and corrosion inhibition investigations. Curr Chem Lett 9:19–30. https://doi.org/10.5267/j.ccl.2019.006.005
18. Savita P, Mourya N, Chaubey S, Kumar VK, Singh M.M, Singh (2016) *Strychnos nuxvomica*, *Piper longum* and *Mucuna pruriens* seed extracts as eco-friendly corrosion inhibitors for copper in nitric acid. RSC Adv. 6:95644–95655. https://doi.org/10.1039/C6RA16481A
19. Bidi MA, Azadi M, Rassouli M (2020) A new green inhibitor for lowering the corrosion rate of carbon steel in 1 M HCl solution: Hyalomma tick extract. Mater Today Commun. https://doi.org/10.1016/j.mtcomm.2020.100996
20. Udensi SC, Ekpe OE, Nnanna LA (2020) *Newbouldia laevis* leaves extract as tenable eco-friendly corrosion inhibitor for aluminium alloy AA7075-T7351 in 1 M HCl corrosive environment: gravimetric, electrochemical and thermodynamic studies. Chem Africa 3:303–316. https://doi.org/10.1007/s42250-020-00131-w
21. Raphael VP, Kakkassery JT, Shanmughan SK, Varghese S (2016) Interaction of two water soluble heterocyclic hydrazones on copper in nitric acid: electrochemical, surface morphological, and quantum chemical investigations. Int J Metals 2016:1–8. https://doi.org/10.1155/2016/6509469
22. Haladu SA, Dalhat Muazu N, Ali SA, Elsharif AM, Odewunmi NA, Abd El-Lateef HM (2022) Inhibition of mild steel corrosion in 1 M H2SO4 by a gemini surfactant 1,6-hexyldiyl-bis-(dimethyldodecylammonium bromide): ANN, RSM predictive modeling, quantum chemical and MD simulation studies. J. Mol. Liq. 350:118533. https://doi.org/10.1016/j.molliq.2022.118533
23. Sharma RP, Madhukesh JK, Shukla S, Prasannakumara BC (2023) Numerical and levenberg–marquardt backpropagation neural networks computation of ternary nanofluid flow across parallel plates with Nield boundary conditions. Eur Phys J Plus 138:63. https://doi.org/10.1140/epjp/s13360-023-03680-4
24. Sanni O, Popoola API (2019) Assessment of concentration, temperature and exposure time effect on waste product as a sustainable inhibitor for stainless steel corrosion: optimization using response surface method. J Bio- Tribo-Corros 5:1–14. https://doi.org/10.1007/s40735-019-0239-3
25. Priya RSSV (2019) Corrosion inhibition of mild steel in 1 M HCl and 0.5 M H_2SO_4 by natural product extract—a comparative analysis by electrochemical studies. Int. J. Adv. Res. Chem. Chem. Eng. 1:0–7
26. Joshi V, Bachhar V, Singh P, Duseja M, Haldhar R, Katin KP, Berdimurodov E, Shukla RK (2025) Rheological and anticorrosion study of *Piper chaba* extract and coating for mild steel in 2M H_2SO_4. Colloids Surf A Physicochem Eng Asp 708:135989. https://doi.org/10.1016/j.colsurfa.2024.135989
27. Bachhar V, Joshi V, Singh P, Berisha A, Haldhar R, Duseja M, Shukla R (2024) Anticorrosion and rheological properties of *Calyptocarpus vialis* extract as a green coating for mild steel in 2M H_2SO_4. Colloids Surfaces A Physicochem Eng Asp 705:135606. https://doi.org/10.1016/j.colsurfa.2024.135606
28. Haldhar R, Raorane CJ, Bachhar V, Katin KP, Berdimurodov E, Shazly GA, Kim S-C (2025) Dual-functional *Quercus palustris*

leaves extract as a sustainable corrosion inhibitor for low-carbon steel and its biomedical potential: electrochemical, biological, and computational insights. Sustain Mater Technol 44:e01378
29. Anupama KK, Joseph A (2018) Experimental and theortical studies on *Cinnamomum verum* leaf extract and one of its major components, Eugenol as environmentally benign corrosion inhibitors for mild steel in acid media. J Bio- Tribo-Corros. https://doi.org/10.1007/s40735-018-0146-z
30. Tsoeunyane MG, Makhatha ME, Arotiba OA (2019) Corrosion inhibition of mild steel by Poly(butylene succinate)-L-histidine extended with 1,6-diisocynatohexane polymer composite in 1 M HCl. Int J Corros. https://doi.org/10.1155/2019/7406409
31. Dagdag O, Safi Z, Erramli H, Wazzan N, Guo L, Verma C, Ebenso EE, Kaya S, El Harfi A (2020) Epoxy prepolymer as a novel anticorrosive material for carbon steel in acidic solution: electrochemical, surface and computational studies. Mater Today Commun. https://doi.org/10.1016/j.mtcomm.2019.100800
32. Kooliyat R, Kakkassery JT, Raphael VP, Cheruvathur SV, Paulson BM (2019) Synthesis, cyclic voltammetric, electrochemical, and gravimetric corrosion inhibition investigations of Schiff base derived from 5,5-dimethyl-1,3-cyclohexanedione and 2-aminophenol on mild steel in 1 M HCl and 0.5 M H2SO4. Int J Electrochem 2019:1–13. https://doi.org/10.1155/2019/1094148
33. De Lima KCDS, Paiva VM, Perrone D, Ripper B, Simões G, Rocco MLM, Da Veiga AG, D'Elia E (2020) Glycine max meal extracts as corrosion inhibitor for mild steel in sulphuric acid solution. J Mater Res Technol 9:12756–12772. https://doi.org/10.1016/j.jmrt.2020.09.019
34. Aljourani J, Golozar MA, Raeissi K (2010) The inhibition of carbon steel corrosion in hydrochloric and sulfuric acid media using some benzimidazole derivatives. Mater Chem Phys 121:320–325. https://doi.org/10.1016/j.matchemphys.2010.01.040
35. Muthamma K, Kumari P, Lavanya M, Rao SA (2021) Corrosion inhibition of mild steel in acidic media by N- [(3,4-dimethoxyphenyl)methyleneamino]-4-hydroxy-benzamide. J Bio- Tribo-Corrosion 7:1–19. https://doi.org/10.1007/s40735-020-00439-7
36. Mei B-A, Munteshari O, Lau J, Dunn B, Pilon L (2017) Physical interpretations of Nyquist plots for EDLC electrodes and devices. J Phys Chem C. https://doi.org/10.1021/acs.jpcc.7b10582
37. Singh A, Caihong Y, Yaocheng Y, Soni N, Wu Y, Lin Y (2019) Analyses of new electrochemical techniques to study the behavior of some corrosion mitigating polymers on N80 tubing steel. ACS Omega 4:3420–3431. https://doi.org/10.1021/acsomega.8b02983
38. Loto RT, Loto CA, Fedotova T (2014) Electrochemical studies of mild steel corrosion inhibition in sulfuric acid chloride by aniline. Res Chem Intermed 40:1501–1516. https://doi.org/10.1007/s11164-013-1055-x
39. Majd MT, Ramezanzadeh M, Ramezanzadeh B, Bahlakeh G (2020) Production of an environmentally stable anti-corrosion film based on Esfand seed extract molecules-metal cations: integrated experimental and computer modeling approaches. J Hazard Mater. https://doi.org/10.1016/j.jhazmat.2019.121029
40. Ameer M, Fekry A (2011) Corrosion inhibition of mild steel by natural product compound. Prog Org Coat 71:343–349. https://doi.org/10.1016/j.porgcoat.2011.04.001
41. Mehdipour M, Ramezanzadeh B, Arman SY (2015) Electrochemical noise investigation of Aloe plant extract as green inhibitor on the corrosion of stainless steel in 1M H_2SO_4. J Ind Eng Chem 21:318–327. https://doi.org/10.1016/j.jiec.2014.02.041
42. Wei Z, Goehring T, Mioduszewski M, Luo L, Kotrba A, Rybarz M, Ellinghaus K, Pieszkalla M (2016) Failure mechanisms and modes analysis of vehicle exhaust components and systems. In: Handbook of materials failure analysis with case studies from the aerospace and automotive industries. Boston, pp 393–432. https://doi.org/10.1016/B978-0-12-800950-5.00018-1
43. Haldhar R, Prasad D, Saxena A, Kumar R (2018) Experimental and theoretical studies of *Ficus religiosa* as green corrosion inhibitor for mild steel in 0.5 M H_2SO_4 solution. Sustain Chem Pharm 9:95–105. https://doi.org/10.1016/j.scp.2018.07.002
44. Allal H, Belhocine Y, Emna Z (2018) Computational study of some thiophene derivatives as aluminium corrosion inhibitors. J Mol Liq. https://doi.org/10.1016/j.molliq.2018.05.099
45. Agu CM, Menkiti MC, Ekwe EB, Agulanna AC (2020) Modeling and optimization of *Terminalia catappa* L. kernel oil extraction using response surface methodology and artificial neural network. Artif Intell Agric 4:1–11. https://doi.org/10.1016/j.aiia.2020.01.001
46. Olawale O, Bello JO, Ogunsemi BT, Uchella UC, Oluyori AP, Oladejo NK (2019) Optimization of chicken nail extracts as corrosion inhibitor on mild steel in 2M H2SO4. Heliyon. https://doi.org/10.1016/j.heliyon.2019.e02821
47. Sabu AS, Mathew A, Neethu TS et al (2021) Statistical analysis of MHD convective ferro-nanofluid flow through an inclined channel with hall current, heat source and Soret effect. Therm. Sci. Eng. Prog. 22:100816. https://doi.org/10.1016/j.tsep.2020.100816
48. Prabhu PR, Prabhu D, Rao P (2020) Analysis of *Garcinia indica* Choisy extract as eco-friendly corrosion inhibitor for aluminum in phosphoric acid using the design of experiment. J Mater Res Technol 9:3622–3631. https://doi.org/10.1016/j.jmrt.2020.01.100
49. Mehmood T, Ramzan M, Howari F, Kadry S, Chu Y-M (2021) Application of response surface methodology on the nanofluid flow over a rotating disk with autocatalytic chemical reaction and entropy generation optimization. Sci Rep. https://doi.org/10.1038/s41598-021-81755-x